Circulation Research

American Heart Association®

Loss of Angiotensin-Converting Enzyme-2 Exacerbates Diabetic Cardiovascular Complications and Leads to Systolic and Vascular Dysfunction : A Critical Role of the Angiotensin II/AT1 Receptor Axis

Vaibhav B. Patel, Sreedhar Bodiga, Ratnadeep Basu, Subhash K. Das, Wang Wang, Zuocheng Wang, Jennifer Lo, Maria B. Grant, JiuChang Zhong, Zamaneh Kassiri and Gavin Y. Oudit

The online version of this article, along with updated information and services, is located on the World Wide Web at:

http://circres.ahajournals.org/content/110/10/1322

Data Supplement (unedited) at:

http://circres.ahajournals.org/content/suppl/2012/04/03/CIRCRESAHA.112.268029.DC1.html

---

Permissions: Requests for permissions to reproduce figures, tables, or portions of articles originally published in *Circulation Research* can be obtained via RightsLink, a service of the Copyright Clearance Center, not the Editorial Office. Once the online version of the published article for which permission is being requested is located, click Request Permissions in the middle column of the Web page under Services. Further information about this process is available in the Permissions and Rights Question and Answer document.

Reprints: Information about reprints can be found online at:
http://www.lww.com/reprints

Subscriptions: Information about subscribing to *Circulation Research* is online at:
http://circres.ahajournals.org//subscriptions/

Loss of Angiotensin-Converting Enzyme-2 Exacerbates Diabetic Cardiovascular Complications and Leads to Systolic and Vascular Dysfunction
A Critical Role of the Angiotensin II/AT1 Receptor Axis

Vaibhav B. Patel, Sreedhar Bodiga, Ratnadeep Basu, Subhash K. Das, Wang Wang, Zuocheng Wang, Jennifer Lo, Maria B. Grant, JiuChang Zhong, Zamaneh Kassiri, Gavin Y. Oudit

Rationale: Diabetic cardiovascular complications are reaching epidemic proportions. Angiotensin-converting enzyme-2 (ACE2) is a negative regulator of the renin-angiotensin system. We hypothesize that loss of ACE2 exacerbates cardiovascular complications induced by diabetes.

Objective: To define the role of ACE2 in diabetic cardiovascular complications.

Methods and Results: We used the well-validated Akita mice, a model of human diabetes, and generated double-mutant mice using the ACE2 knockout (KO) mice (Akita/ACE2$^{-/y}$). Diabetic state was associated with increased ACE2 in Akita mice, whereas additional loss of ACE2 in these mice leads to increased plasma and tissue angiotensin II levels, resulting in systolic dysfunction on a background of impaired diastolic function. Downregulation of SERCA2 and lipotoxicity were equivalent in Akita and Akita/ACE2KO hearts and are likely mediators of the diastolic dysfunction. However, greater activation of protein kinase C and loss of Akt and endothelial nitric oxide synthase phosphorylation occurred in the Akita/ACE2KO hearts. Systolic dysfunction in Akita/ACE2KO mice was linked to enhanced activation of NADPH oxidase and metalloproteinases, resulting in greater oxidative stress and degradation of the extracellular matrix. Impaired flow-mediated dilation in vivo correlated with increased vascular oxidative stress in Akita/ACE2KO mice. Treatment with the AT1 receptor blocker, irbesartan rescued the systolic dysfunction, normalized altered signaling pathways, flow-mediated dilation, and the increased oxidative stress in the cardiovascular system.

Conclusions: Loss of ACE2 disrupts the balance of the renin-angiotensin system in a diabetic state and leads to an angiotensin II/AT1 receptor-dependent systolic dysfunction and impaired vascular function. Our study demonstrates that ACE2 serves as a protective mechanism against diabetes-induced cardiovascular complications. (***Circ Res***. 2012;110:1322-1335.)

Key Words: angiotensin II ■ angiotensin-converting enzyme-2 ■ AT1 receptor ■ diabetes ■ renin angiotensin system

Diabetes mellitus results in severe cardiovascular complications, and heart disease and failure remain the major causes of death in patients with diabetes.[1–5] Given the increasing global tide of obesity and diabetes, the clinical burden of diabetes-induced cardiovascular disease is reaching epidemic proportions. Diabetic cardiomyopathy refers to ventricular dysfunction that occurs in the absence of any changes in blood pressure and coronary artery disease, with phenotypic features such as cardiomyocyte apoptosis, cardiac hypertrophy, myocardial fibrosis, and interstitial inflammation.[4,6,7] Several key mechanisms have been proposed and tested to explain diabetic myocardial dysfunction, some of which include increased oxidative stress, impaired calcium homeostasis, upregulation of the renin-angiotensin system (RAS), lipotoxicity, and mitochondrial dysfunction.[4,6]

Activation of the RAS plays a key role in the progression of diabetic complications and AT1 receptor blockers have reduced

these complications.[8–11] Angiotensin-converting enzyme-2 (ACE2) is a carboxypeptidase that metabolizes angiotensin II (Ang II) to yield angiotensin 1 to 7 (Ang 1–7), essentially negatively regulating the RAS.[12–15] We hypothesized that loss of ACE2 accelerates diabetic injury in the cardiovascular system. We investigated cardiac and vascular structure and function, Ang II metabolism, signaling, and tissue reactive oxygen species generation in insulin-deficient diabetic Akita mice in response to genetic ablation of ACE2. In this study, we demonstrate that loss of ACE2 mediates development of systolic dysfunction and impaired vascular function in Akita mice. We identified augmented superoxide production, activation of the extracellular matrix (ECM)-degrading metalloproteinases, and differential signaling as the underlying mechanisms in this model of diabetic cardiovascular injury.

Methods

Experimental Animals and Protocol

C57BL/6J wild-type (WT) and diabetic heterozygous Akita ($Ins2^{WT/C96Y}$) and db/db mice were purchased from The Jackson Laboratory (Bar Harbor, ME). Male Akita mice were bred with female WT mice at the University of Alberta animal facility. Similarly, male heterozygous Akita mice were crossed with female ACE2$^{-/-}$ mutant mice (ACE2KO) to obtain Akita/ACE2KO ($Ins2^{WT/C96Y}$/ACE2$^{-/y}$) double mutants (Detailed Methods are provided in the Online Supplement.). Throughout the period of study, animals were provided free access to water and standard 18% protein rodent chow (Harlan Teklad). A subgroup of Akita/ACE2KO mice also was treated with irbesartan, an AT1 receptor blocker (50 mg/kg^{-1}/d^{-1}) or Ang 1–7 (24 μg/kg/h; Bachem) for 1 month starting at 5 months of age. A subgroup of Akita mice was also treated with irbesartan (50 mg/kg^{-1}/d^{-1}) for 1 month starting at 5 months of age. The use of animals in this study conforms to the Care and Use of Laboratory Animals published by the United States National Institutes of Health (NIH Publication 85-23, revised 1996) and to the guidelines of the Canadian Council on Animal Care.

Echocardiography and Tissue Doppler Imaging

Transthoracic echocardiography was performed noninvasively to assess systolic and diastolic functions as described previously using a Vevo 770 high-resolution imaging system equipped with a 30-MHz transducer (RMV-707B; VisualSonics).[13,16]

Tail-Cuff Systolic Blood Pressure Measurements

Systolic blood pressure of each mouse was measured by the tail-cuff method with an IITC blood pressure monitoring system (IITC Life Science) as previously described.[13]

Assessment of Flow-Mediated Vasodilation

Six-month-old male WT, Akita, ACE2KO, and Akita/ACE2KO and irbesartan-treated Akita/ACE2KO mice were anesthetized with isoflurane (2% induction and 1% maintenance), and body temperature was maintained at 36.9°C to 37°C. A 40-MHz transducer (RMV-704; Visual Sonics) was used to visualize the left femoral artery. The left femoral artery was identified on the basis of its characteristic flow pattern.[17] Doppler flow measurements from longitudinal sections of the femoral artery were obtained before and after 5 minutes of hind limb ischemia. Reproducible ischemia (seen as complete abrogation of Doppler flow wave) and reperfusion of the hind limb (reappearance of Doppler flow waveforms after 5 minutes of ischemia) were achieved with a traction suture as an arterial loop occluder that was positioned upstream of the site to be visualized, around the left common iliac artery, through a transfemoral access. The loop occluder consisted of a 7-0 nylon filament around the artery that was externalized and skin was closed with suture. Baseline readings were recorded after a 10-minute equilibration period followed by complete hind limb ischemia achieved by using the traction

Non-standard Abbreviations and Acronyms	
ACE2	angiotensin-converting enzyme 2
Ang 1-7	angiotensin 1-7
Ang II	angiotensin II
β-MHC	β-myosin heavy chain
BNP	brain natriuretic peptide
DHE	dihydroethidium
ECM	extracellular matrix
eNOS	endothelial nitric oxide synthase
ERK1/2	extracellular signal regulated kinases-1/2
FMD	flow-mediated dilation
JAK2	Janus-activated kinase-2
MMP	matrix metalloproteinase
NO	nitric oxide
NOX2	NADPH oxidase 2
PKC	protein kinase C
PLN	phospholamban
RAS	renin angiotensin system
SERCA2	sarcoplasmic reticulum Ca2+-ATPase2a
STAT3	signal transducer and activator of transcription-3
TIMP	tissue inhibitor of metalloproteinase
TUNEL	terminal deoxynucleotidyl transferase-mediated dUTP nick-end labeling

suture to occlude the common iliac artery. After 5 minutes of ischemia, the hind limb was reperfused by release of the occluder. Reactive hyperemia was measured by Doppler flow velocity of the left femoral artery at reperfusion and at 1, 2, 3, 4, and 5 minutes postreperfusion.

Biochemical Measurements

Random blood glucose was measured using Ascensia Contour glucometer (Bayer) as previously described.[16] Identification and quantification of the major long-chain acyl CoA molecular species and myocardial ceramide levels (C18) were performed by high-performance liquid chromatography as previously described.[16] Left ventricular (LV) myocardial ACE2 activity was measured using a specific fluorogenic substrate and calculated as the DX-600 suppressible activity as previously described.[13]

Histological Analyses, TUNEL Assay, and Immunofluorescence

Hearts were arrested in diastole with 1 mol/L KCl, fixed with 10% buffered formalin, and embedded in paraffin. Ten-micrometer-thick sections were stained with picro-sirius red and visualized using fluorescence microscopy as previously described.[13] Myocyte cross-sectional area was measured using wheat germ agglutinin-oregon 488 (Invitrogen) staining in 5-micrometer-thick OCT-embedded cryosections. In situ DNA fragmentation was detected in 15-micrometer-thick cryosections using the commercially available terminal deoxynucleotidyltransferase-mediated dUTP nick-end labeling (TUNEL) assay according to manufacturer's instructions (Invitrogen). Nitrotyrosine immunofluorescence staining was performed in 5-micrometer-thick aorta cryosections using rabbit antinitrotyrosine (Millipore) primary antibody and TRITC-conjugated goat antirabbit (Abcam) secondary antibody.

Real-Time Reverse-Transcriptase Polymerase Chain Reaction and Western Blot Analysis

Myocardial mRNA expression levels were quantified by Taqman reverse-transcriptase polymerase chain reaction (Online Table I) as described previously.[13,16,18] Western blotting was performed to
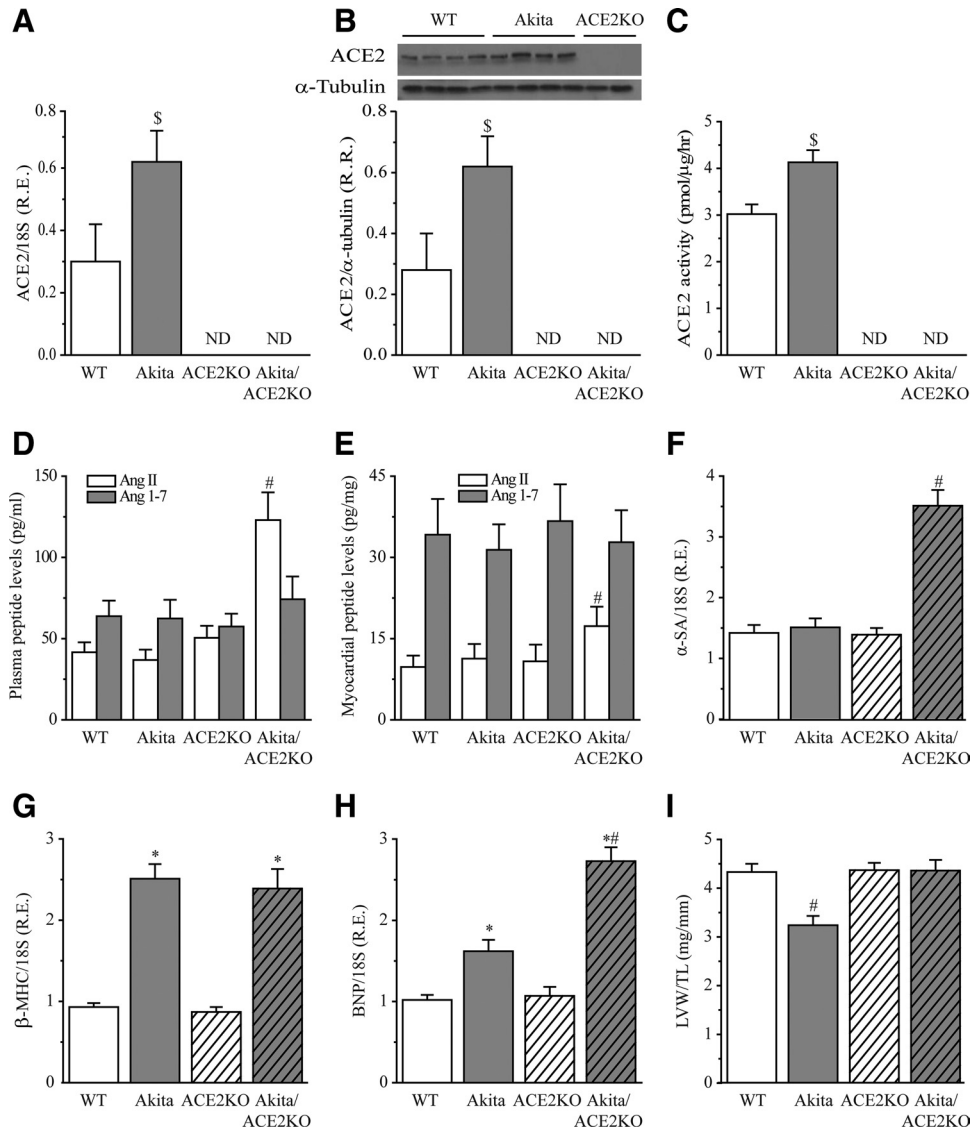
Figure 1. Upregulation of angiotensin-converting enzyme 2 (ACE2) in diabetic hearts, with loss of ACE2 increasing angiotensin (Ang) II levels and activating pathological gene expression. ACE2 mRNA expression (**A**), protein levels (**B**), and ACE2 activity (**C**) are upregulated in Akita hearts, whereas loss of ACE2 in the Akita/ACE2 knockout (KO) increases plasma (**D**) and myocardial (**E**) Ang II levels and is associated with increased α-skeletal actin (α-SA) (**F**), β-myosin heavy chain (β-MHC) (**G**), and brain-type natriuretic peptide (BNP) (**H**) expression in the heart in the absence of overt hypertrophy (**I**). ND, not detectable; LVW, left ventricular weight; TL, tibial length; RE, relative expression; RR, relative ratio; n=6 (**A–C**), n=15 (**D, E**), and n=10 (**F–I**). $P<0.05 compared to the wild-type (WT) group. *$P<0.05$ for the main effects and #$P<0.05$ for the interaction using two-way ANOVA.

detect ACE2, protein kinase Cα (PKCα), phosphorylated and total levels of Akt (serine-473 and threonine-308), JAK2 (tyrosine-1007/1008), STAT3 (tyrosine-705), ERK-1/2 (threonine-177), and endothelial nitric oxide synthase (eNOS; serine-1177) using specific antibodies (Cell Signaling), pyruvate dehydrogenase-4 (Abgent Canada), and, for SERCA2a, phospho (serine 16)-phospholamban and total phospholamban (Santa Cruz), as previously described.[13,16,18] Blots were scanned and quantified using ImageQuant LAS 4000 (GE Healthcare, Biosciences).

Plasma and Myocardial Peptide Levels

Plasma and LV myocardial Ang II and Ang 1–7 levels were measured at the Hypertension Core Laboratory, Wake Forest University, Winston-Salem, North Carolina, as previously described.[13,14]

Gelatin Zymography, Collagenase, and Gelatinase Activity

Gelatin zymography was performed as previously described.[12] Total collagenase and gelatinase activities were measured using fluores-

cent-based activity assays from EnzCheck (Molecular Probes) as described previously.[19,20] Samples were analyzed using a Spectra-Max M5 microplate reader (Molecular Devices).

Superoxide Assay and Dihydroethidium Staining

The chemiluminescence lucigenin assay was used to measure NADPH oxidase activity as we have previously described.[13,14] The specific peptide inhibitor of NADPH oxidase, gp91phox ds tat (50 μmol/L), was used to confirm superoxide generation from NADPH oxidase.[13,14] Dihydroethidium (DHE) fluorescence studies were performed on 20-micrometer-thick frozen myocardial sections, which were washed with Hank's balanced salt solution incubated at 37°C for 30 minutes with DHE (20 μmol/L) in Hank's balanced salt solution, and then imaged using confocal microscopy.

Statistical Analysis

Comparison between two groups was made using a nonpaired Student t test (Figure 1A–C; Online Figure IA, E). Two-way
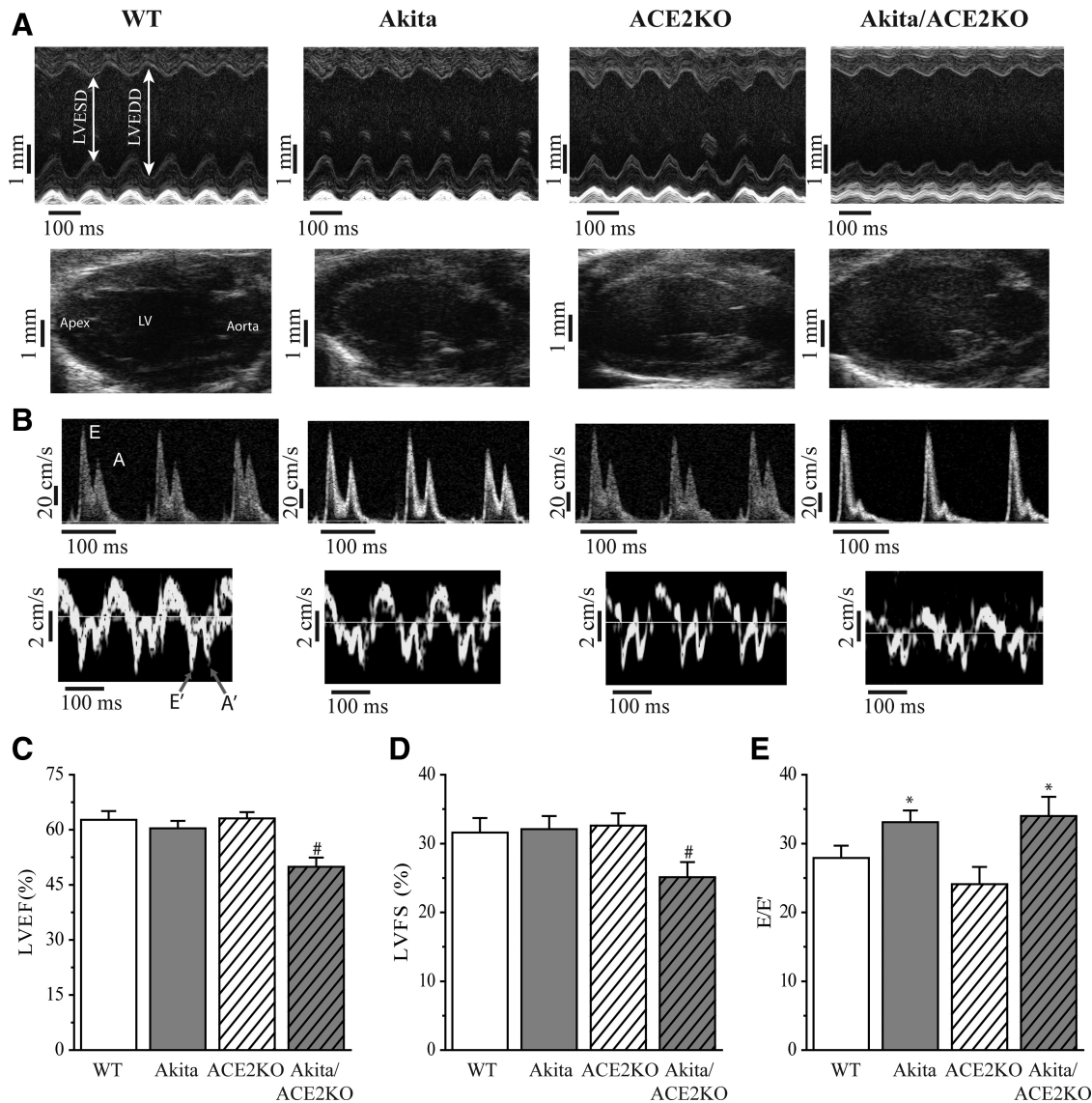
Figure 2. Loss of angiotensin-converting enzyme 2 (ACE2) leads to systolic dysfunction in diabetic Akita mice. Echocardiographic assessment of heart function showing M-mode images and parasternal long-axis views (**A**) and transmitral flow pattern and tissue Doppler imaging (**B**) showing systolic dysfunction in Akita/ACE2 knockout (KO) hearts within a background of diastolic dysfunction in the Akita hearts. Quantitative evaluation of systolic function showing reduction in left ventricular (LV) ejection fraction (LVEF) (**C**) and LV fractional shortening (LVFS) (**D**) in Akita/ACE2KO mice coupled with equivalent diastolic dysfunction illustrated by elevation of the E/E′ ratio (**E**) in Akita and Akita/ACE2KO mice. n=12 for each group. $^{\#}P<0.05$ for the interaction using two-way ANOVA.

ANOVA using diabetic state and ACE2 status as the two independent variables (factors) was performed to compare the data between the four experimental groups (WT, Akita, ACE2KO, and Akita/ACE2KO; Figure 1D–I, Figures 2–6, Online Figure IC, D; II–V, VIA). In experiments with multiple treatments, one-way ANOVA was followed by multiple comparison using the Student Neuman-Keuls test (Figures 7, 8, Online Figure IB, Online Figure VIB–VIII). Statistical analyses were performed using the SPSS Statistics 19 software. Averaged values are presented as means ± SEM. Statistical significance is recognized at $P<0.05$.

Results

Loss of ACE2 Increases Ang II Levels, Activates Pathological Gene Expression, and Leads to Systolic Dysfunction in Diabetic Hearts

Expression analysis and Western blotting showed a significant increase in ACE2 mRNA and protein levels (Figure 1A, B),

resulting in increased ACE2 activity in Akita diabetic hearts (Figure 1C) without changes in ACE2 levels in the kidneys and a concordant increase in ACE2 levels in diabetic db/db hearts (Online Figure IA, B). We hypothesize that upregulation of ACE2 suppressed the activation of the RAS in a diabetic state and, as such, we generated Akita/ACE2KO double-mutant mice to probe the pathophysiological relevance of ACE2. Plasma and myocardial levels of Ang II were similar in WT, Akita, and ACE2KO mice, whereas Akita/ACE2KO mice showed significantly higher levels confirming activation of the RAS (Figure 1D, E). Interestingly, plasma and myocardial levels of Ang 1–7 were similar across all four experimental groups (Figure 1D, E). Loss of ACE2 conceivably could lead to differential impact on hyperglycemia and blood pressure. However, we found a markedly sustained and equivalent hyperglycemia in Akita and
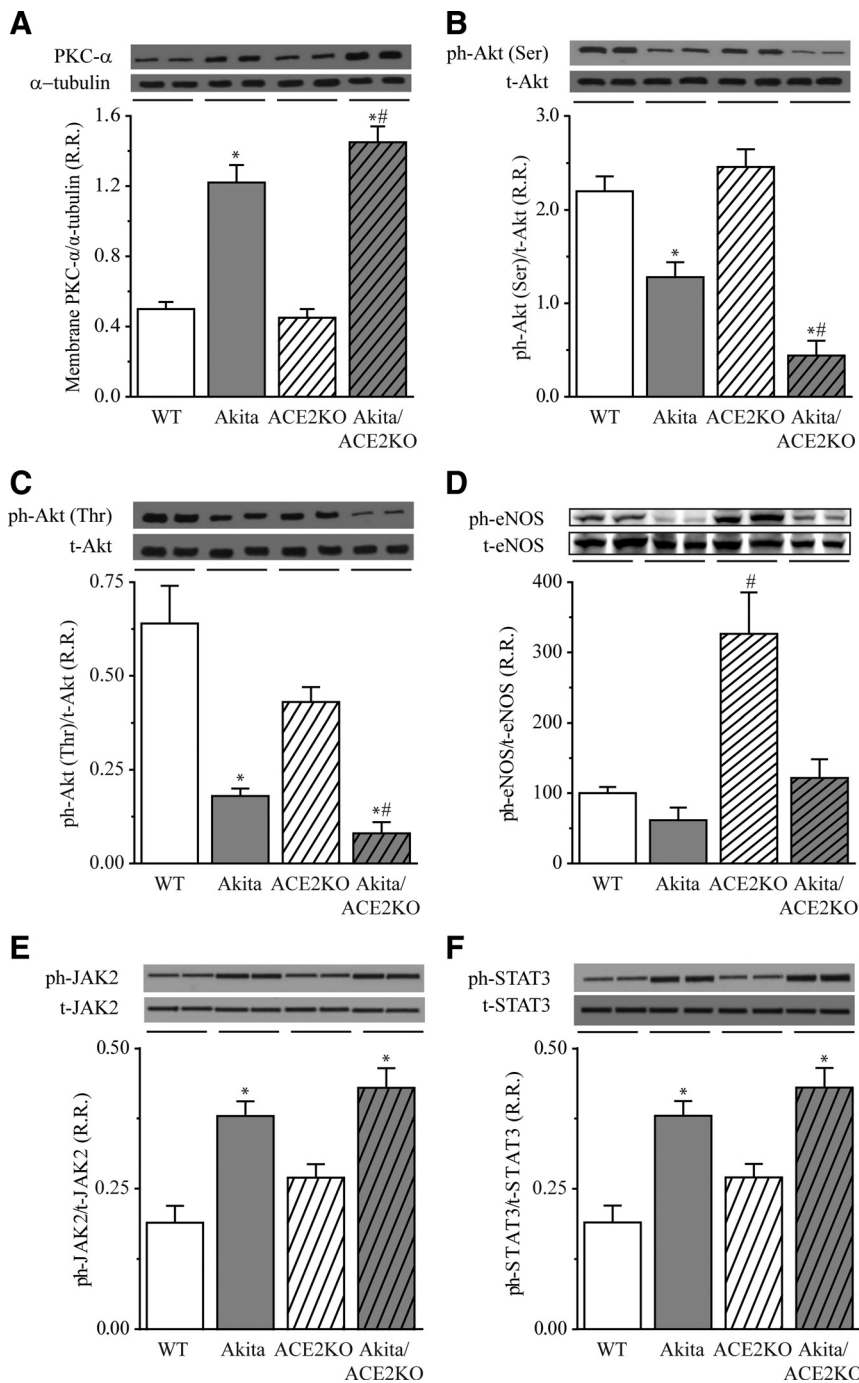
Figure 3. Activation of signaling pathways in Akita and Akita/angiotensin-converting enzyme 2 (ACE2) knockout (KO) hearts. Western blot analysis of protein kinase C (PKC-α) (**A**) and phosphorylation of serine-473 Akt (**B**) and threonine-308 Akt (**C**) showing greater increase in PKC-α and a greater loss of Akt phosphorylation in Akita/ACE2KO hearts compared with Akita hearts. Western blot analysis of phospho and total endothelial nitric oxide synthase (eNOS) (**D**) showed a significant increase in ACE2KO hearts, which was lost in the Akita/ACE2KO hearts. Western blot analysis of phospho and total Janus-activated kinase-2 (JAK2) (**E**) and signal transducer and activator of transcription-3 (STAT3) (**F**) showed equivalent elevation in Akita and Akita/ACE2KO hearts. RR, relative ratio; ph, phosphorylated; t, total. n=5 for each group. *$P<0.05$ for the main effects and #$P<0.05$ for the interaction using two-way ANOVA.

Akita/ACE2KO mice at 3 and 6 months of age and in 6-month old db/db mice (Online Figure IC–E). Similarly, systolic blood pressure was comparably elevated in Akita and Akita/ACE2KO mice with a mild reduction in body weight (Online Figure IIA–C). Ang II is a well-known mediator of pathological remodeling in the heart[13,21] and myocardial expression of α-skeletal actin, β-MHC, and BNP were increased in Akita/ACE2KO mice (Figure 1F–H), indicating pathological changes in the absence of overt hypertrophy based on morphometry and myocyte cross-sectional area (Figure 1I, Online Figure IID, E). These results illustrate that ACE2 is upregulated in diabetic hearts and loss of ACE2 results in increased Ang II levels and

pathological myocardial gene expression without a differential effect on hyperglycemia or blood pressure.

The Akita mouse is a well-characterized nonobese model of type 1 diabetes and closely mimics the human diabetic condition.[16,22,23] WT, Akita, and ACE2KO mice at 6 months of age showed comparable and normal systolic function (Figure 2A, B and Online Table II). In contrast, LV fractional shortening (Figure 2C) and LV ejection fraction (Figure 2D) declined significantly in Akita/ACE2KO mice, indicating LV systolic dysfunction with mild LV dilation (Figure 2 and Online Table II). Tissue Doppler imaging is a novel technique to assess diastolic function and showed a reduction in E′ and E′/A′ ratio
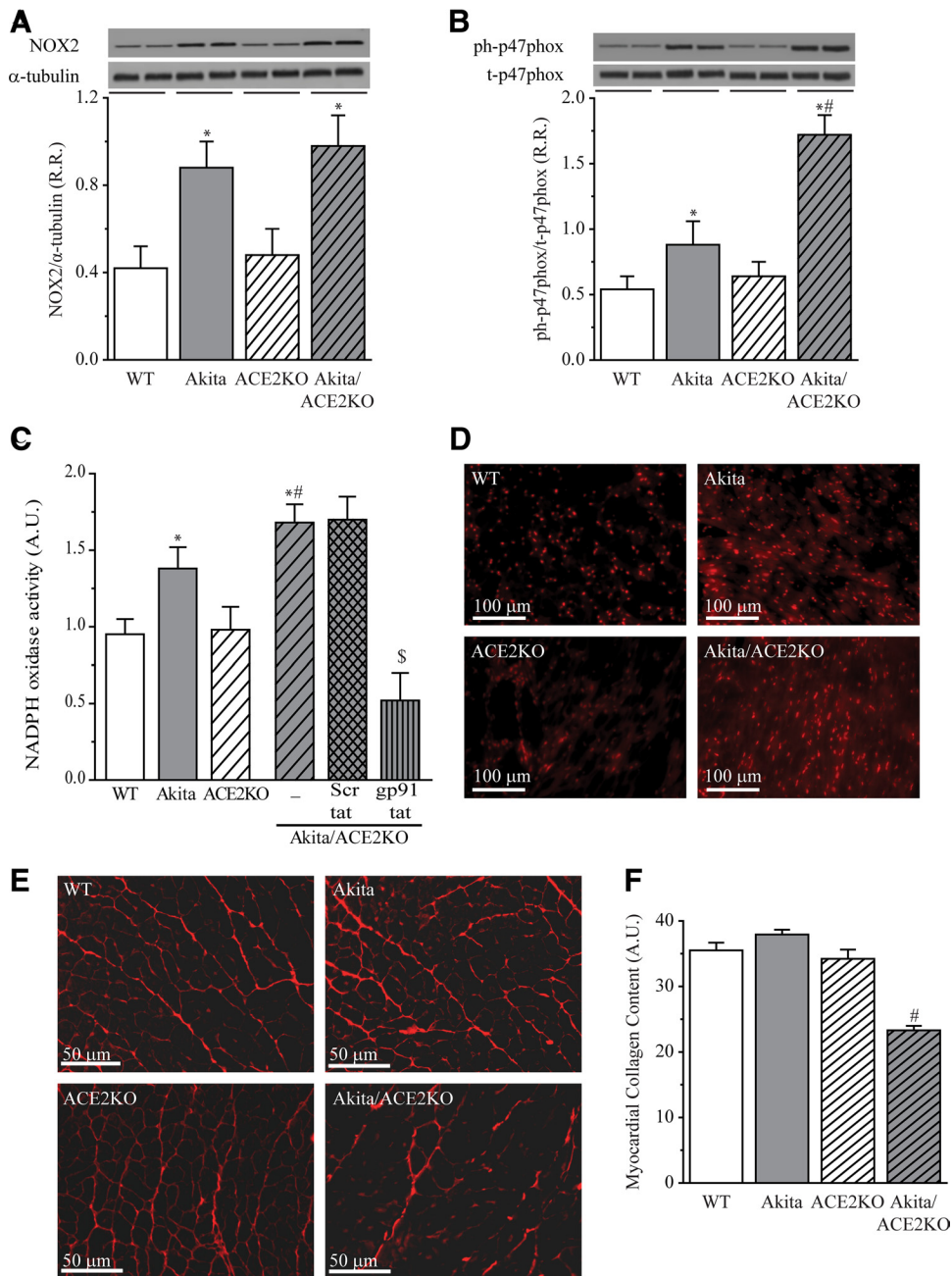
Figure 4. Increased activation of the NADPH oxidase system and degradation of the extracellular matrix in Akita/angiotensin-converting enzyme 2 (ACE2) knockout (KO) hearts. Increased NOX2 levels (**A**) and phosphorylation of the p47phox subunit (**B**), resulting in increased NADPH oxidase activity (**C**) in Akita hearts, with a greater increase in Akita/ACE2KO hearts, which was confirmed by dihydroethidium (DHE) staining showing greater superoxide generation in Akita/ACE2KO hearts (**D**). Picro-sirius red (PSR) staining and imaging using fluorescence microscopy showing intact and organized extracellular matrix (ECM) in wild-type (WT), Akita, and ACE2KO hearts and a degraded and disorganized ECM in the Akita/ACE2KO heart (**E**). Morphometric quantification of picro-sirius red staining showed decreased myocardial collagen content in Akita/ACE2KO hearts compared to all other hearts (**F**) (n=3 sections from each heart). The specificity of NADPH oxidase in contributing to the chemiluminescence was verified by using gp91phox ds tat and scr ds tat peptides (**D**). RR, relative ratio; AU, arbitrary unit. n=5 for each group except for (**C**), in which n=8 for each group. *$P<0.05$ for the main effects and #$P<0.05$ for the interaction using two-way ANOVA. $$P<0.05$ compared to the Akita/ACE2KO group with the scrambled peptide (Scr tat).

and elevation in E/E′ that, coupled with enlarged left atrial size, are indicative of elevated LV filling pressure and diastolic dysfunction in Akita and Akita/ACE2KO hearts (Figure 2 and Online Table II). The progressive nature of the cardiomyopathy in Akita/ACE2KO hearts resulted in a restrictive filling pattern with elevated E/A ratio and reduced isovolumetric relaxation time (Figure 2B and Online Table II). These data indicate that in a diabetic state, loss of ACE2 results in systolic dysfunction in a background of diastolic dysfunction.

Pathological Signaling, Lipotoxicity, and Downregulation of SERCA2

Activation of PKC plays a fundamental role in mediating the pathological effects associated with a hyperglycemia diabetic
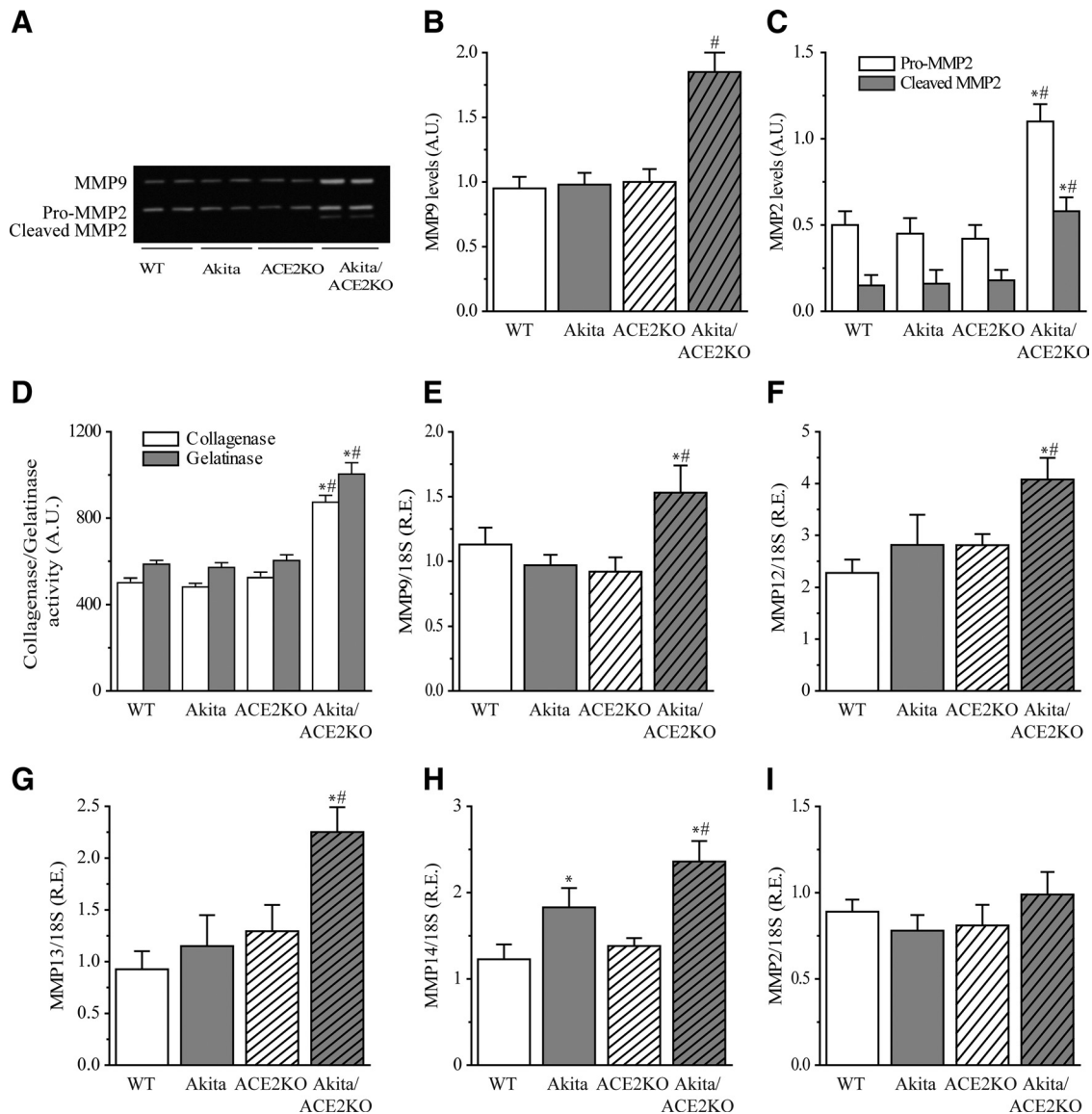
Figure 5. Loss of angiotensin-converting enzyme 2 (ACE2) triggers greater activation of the metalloproteinases in the Akita hearts. Gelatin zymography shows greater levels of matrix metalloproteinase (MMP) 9 (**A**), which is quantified and shown (**B**) with greater pro-MMP2 and active MMP2 levels (**C**) in the Akita/ACE2 knockout (KO) hearts. Gelatinase and collagenase activities showing elevated activity in Akita/ACE2KO hearts in the absence of detectable changes in wild-type (WT), Akita, and ACE2KO hearts (**D**). Expression analysis of mRNA levels showing elevated MMP9 (**E**), MMP12 (**F**), MMP13 (**G**), and MMP14 (MT1-MMP) (**H**) expression, with no detectable change in MMP2 mRNA levels (**I**) in Akita/ACE2KO hearts. AU, arbitrary unit; RE, relative expression. n=10 for each group except for (**A–C**), in which n=5. *$P<0.05$ for the main effects and #$P<0.05$ for the interaction using two-way ANOVA.

state,[24–26] whereas insulin and Ang II activates ERK1/2, PI3K/ Akt, and eNOS signaling cascades in the myocardium.[27–29] To elucidate the basis of the systolic dysfunction in Akita/ ACE2KO hearts, we chose to study the activation of these various signaling pathways implicated in the development of cardiomyopathy. PKCα expression is significantly upregulated in Akita and Akita/ACE2KO myocardium, with a greater elevation in the latter group (Figure 3A). Phosphorylation of Akt at the serine-473 (Figure 3B) and threonine-308 (Figure 3C) residues diminished significantly in Akita hearts and, to a greater extent, in Akita/ACE2KO hearts compared to WT and ACE2KO hearts. Phosphorylation of eNOS at serine-1177 residue was drastically increased in ACE2KO hearts but was lost in the Akita/ACE2KO hearts (Figure 3D),

whereas a comparable increase in phosphorylation of Janus-activated kinase-2 (JAK2) and signal transducer and activator of transcription-3 (STAT3; Figure 3E, F) and ERK1/2 (On-line Figure IIIA) were observed in Akita and Akita/ACE2KO hearts. Thus, loss of ACE2 triggers PKCα expression and a greater loss of Akt and eNOS signaling in diabetic hearts.

Lack of insulin action could lead to fatty acid accumulation and lipotoxicity, which has been linked to diastolic dysfunction.[30,31] Myocardial long-chain fatty acid (palmitoyl CoA, oleoyl CoA, stearoyl CoA) and ceramide were elevated by approximately two-fold in the Akita hearts at 6 months and this was not increased further in Akita/ACE2KO hearts (Online Figure IIIB–D). Loss of insulin signaling also was associated with upregulated mRNA and protein levels of
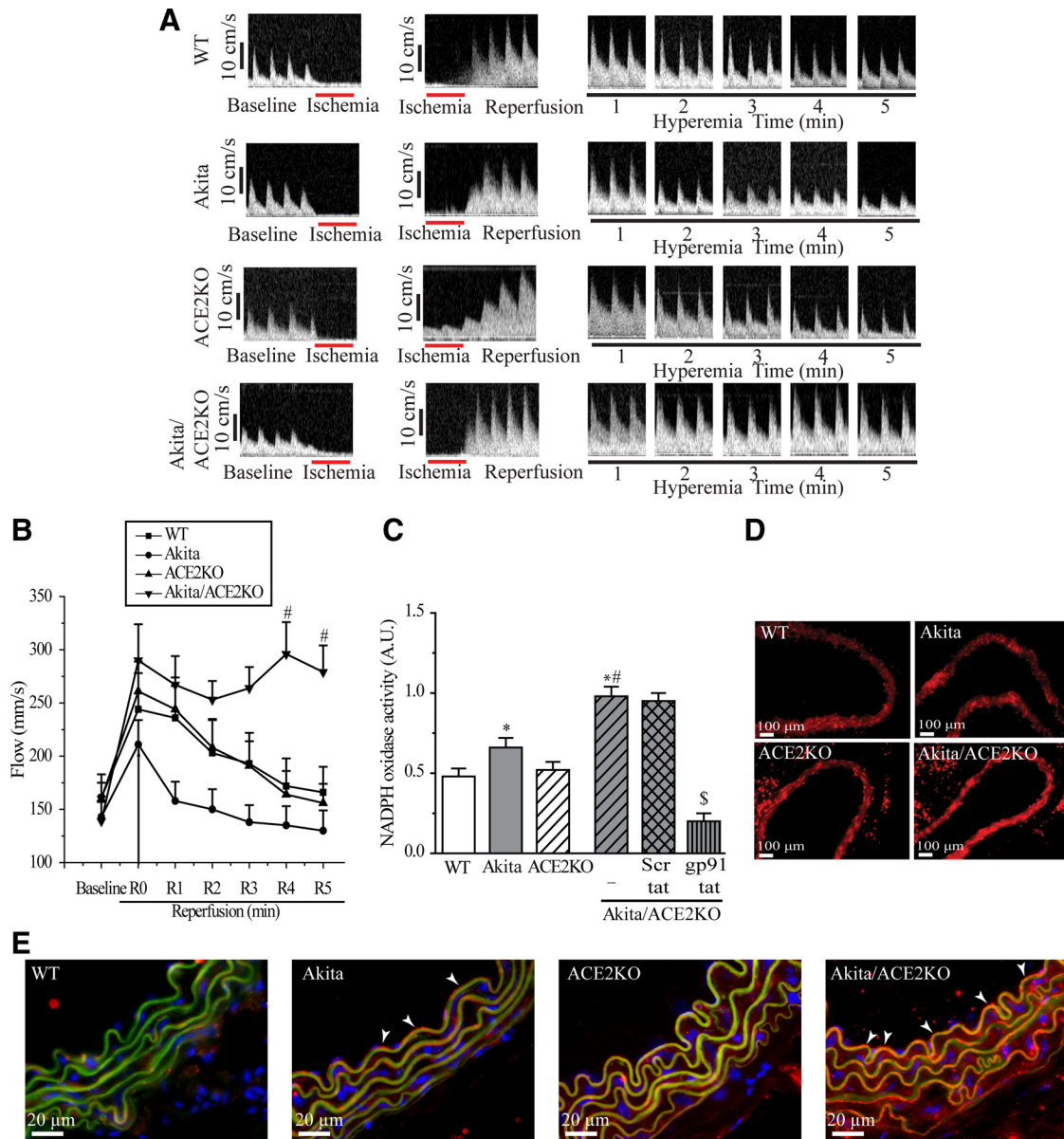
Figure 6. Loss of angiotensin-converting enzyme 2 (ACE2) impaired flow-mediated dilation and activated the vascular NADPH oxidase system. Illustrative images (**A**) and quantification of flow-mediated velocity profile (**B**) in left femoral artery in response to is-chemia-reperfusion showing a marked impairment of the in vivo flow-mediated dilation (FMD) in Akita/ACE2 knockout (KO) mice cou-pled with increased vascular oxidative stress as assessed by NADPH oxidase activity (**C**) and dihydroethidium (DHE) staining (**D**), with **arrow** indicating the start of reperfusion. Representative images of nitrotyrosine immunofluorescence showing increased nitrotyrosine levels in Akita aorta, which further increase in Akita/ACE2KO aorta (**E**), with **arrowheads** indicating nitrotyrosine staining in endothelium in Akita and Akita/ACE2KO aortae (nitrotyrosine [red], elastin autofluorescence [green], and DAPI-stained nuclei [blue]). The specificity of NADPH oxidase in contributing to the chemiluminescence was verified by using gp91phox ds tat and scr ds tat peptides (**C**). n=6 for each group except for (**C**), in which n=12. *$P < 0.05$ for the main effects and #$P < 0.05$ for the interaction using two-way ANOVA. $\$P < 0.05$ compared to the Akita/ACE2KO group with the scrambled peptide (Scr tat).

pyruvate dehydrogenase-4 in Akita hearts (Online Figure IIIE, F). Diastolic dysfunction is linked to suppressed activity of sarcoplasmic reticulum Ca^{2+}-ATPase2a (SERCA2a) pump, which is responsible for the removal of approximately 90% of Ca^{2+} from the cytoplasm.[32,33] SERCA2a expression declined dramatically in both Akita and Akita/ACE2KO compared to WT and ACE2KO, whereas the expression of PLN and phospho-PLN was not altered in any of the experimental groups (Online Figure IVA, B). Analysis of apoptosis showed no significant upregulation of apoptosis in Akita hearts, which was not exacerbated by loss of ACE2

(Online Figure IVC–E). We conclude that the similar extent of lipotoxicity and downregulation of SERCA2a likely un-derlies the comparable diastolic dysfunction in the Akita and Akita/ACE2KO models.

Greater Activation of the NADPH Oxidase and Matrix Metalloproteinases in Akita/ACE2KO Hearts

Hyperglycemia and activation of the RAS are well-known stimulants of the NADPH oxidase system.[13,14,34] Diabetes significantly increased the NADPH oxidase subunit, NOX2,
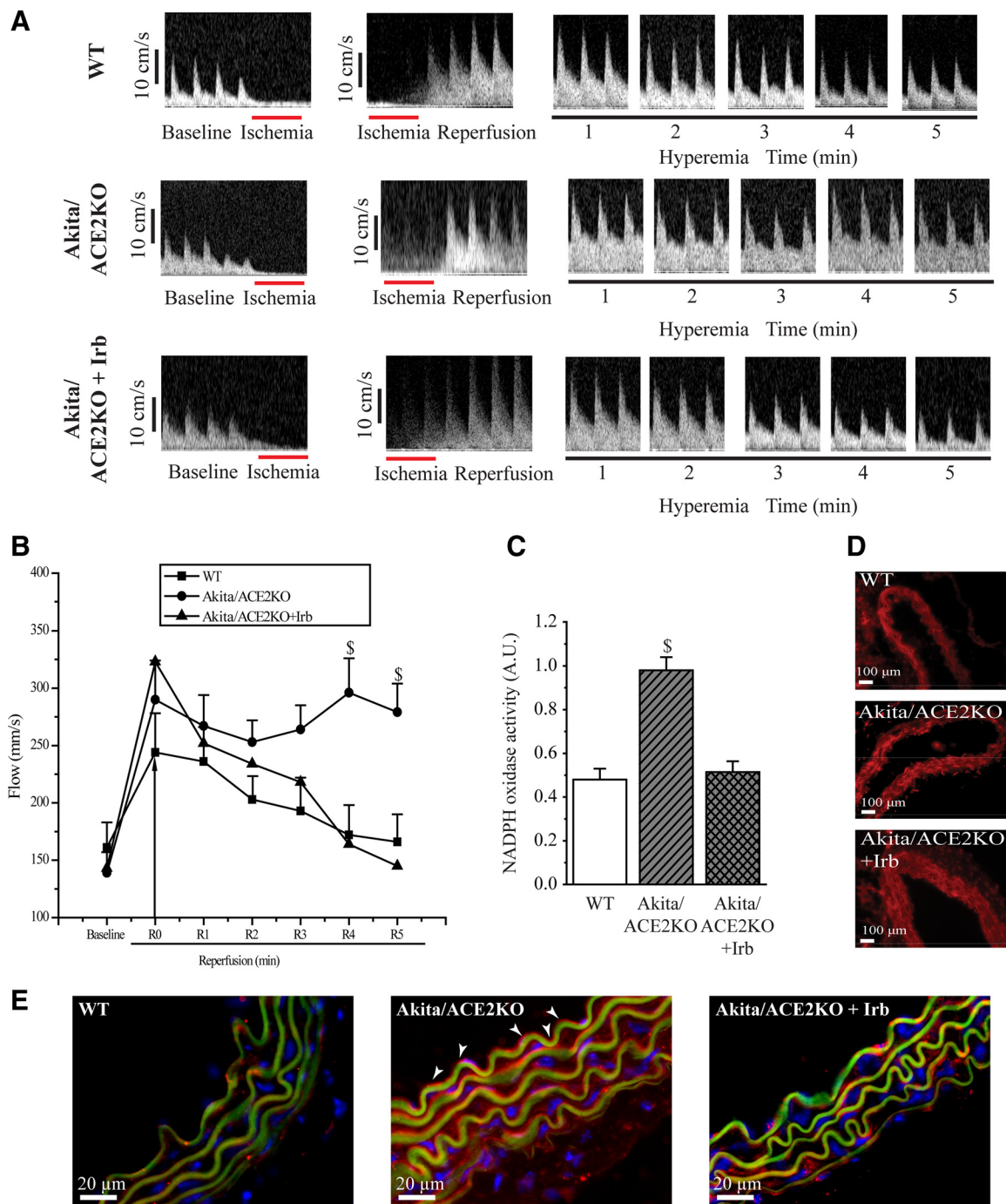
Figure 7. Blockade of AT1 receptor reverses the impairment in flow-mediated dilation and normalizes vascular oxidative stress in Akita/angiotensin-converting enzyme 2 (ACE2) knockout (KO) model. Illustrative images (**A**) and quantification of flow-mediated velocity profile (**B**) in left femoral artery in response to ischemia-reperfusion showing a normalization of the impairment in the in vivo flow-mediated dilation (FMD) in Akita/ACE2KO mice treated with irbesartan. **Arrow** indicates the start of reperfusion. Vascular oxidative stress as assessed by NADPH oxidase activity (**C**) and superoxide level-based dihydroethidium (DHE) fluorescence (**D**) showed a complete suppression of the elevated oxidative stress in the Akita/ACE2KO aorta in response to AT1 receptor blockade. Representative images of nitrotyrosine immunofluorescence showing attenuation of the elevated nitrotyrosine level in Akita/ACE2KO aorta in response to irbesartan treatment (**E**), with **arrowheads** indicating nitrotyrosine staining in the endothelium (nitrotyrosine [red], elastin autofluorescence [green], and DAPI-stained nuclei [blue]). n=8 for each group. $^{\$}P<0.05$ compared to all other groups.

levels in the heart (Figure 4A). Phosphorylation of the p47^{phox} subunit, a key mediator of Ang II–induced NADPH oxidase activation,[14,35] was approximately two-fold higher in Akita myocardium and was further exaggerated in Akita/ACE2KO hearts (Figure 4B). In line with these findings, NADPH oxidase activity was significantly higher in Akita/

ACE2KO hearts, resulting in enhanced superoxide generation, as assessed by lucigenin-enhanced chemiluminescence (Figure 4C) and DHE staining for superoxide levels (Figure 4D). NADPH oxidase activity and DHE fluorescence intensity were increased further in Akita/ACE2KO compared to Akita hearts. The specificity of NADPH oxidase activity was
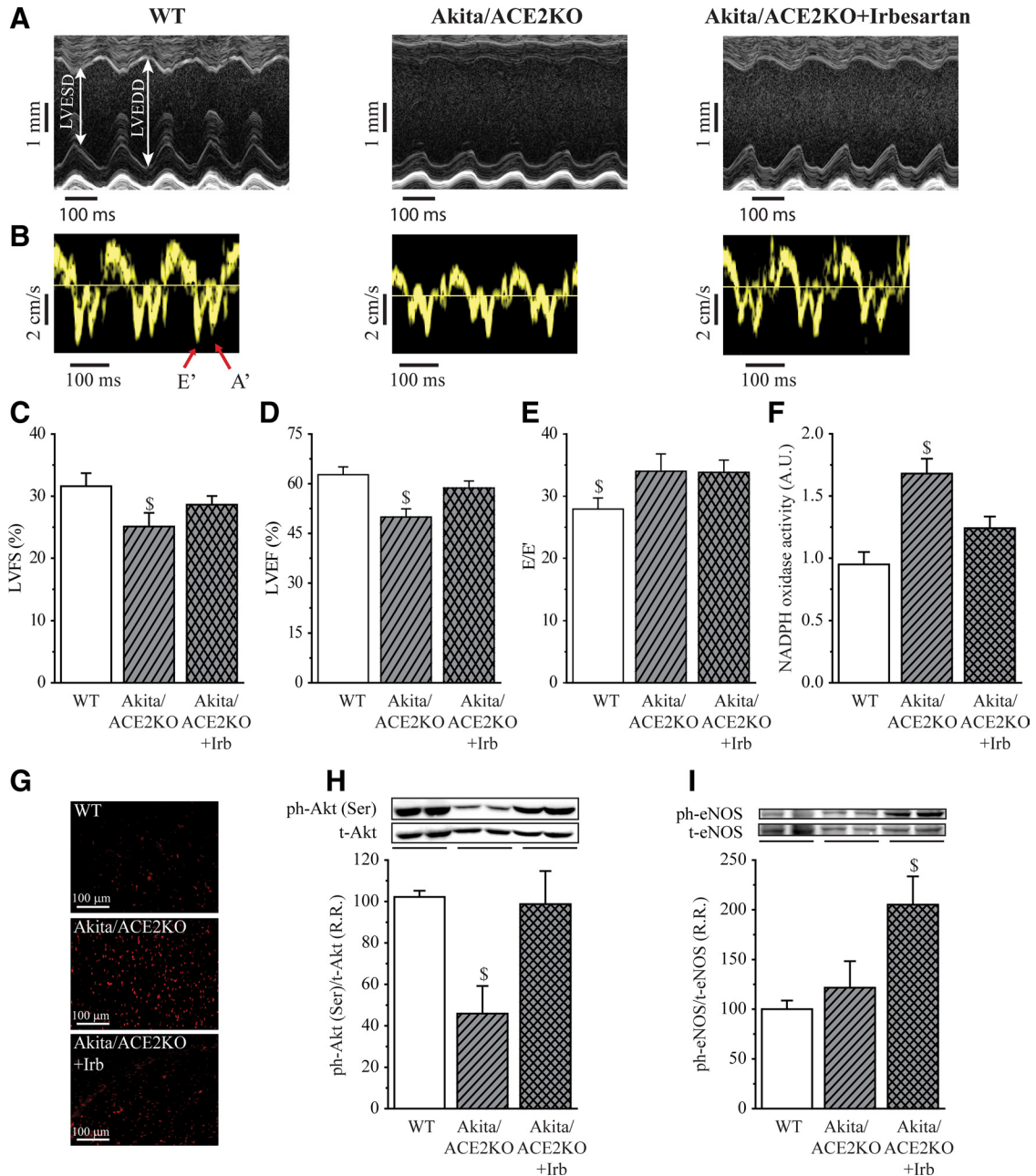
Figure 8. AT1 receptor blockade rescues the systolic dysfunction, suppresses superoxide production, and activates phosphorylation of Akt and endothelial nitric oxide synthase (eNOS) in Akita/angiotensin-converting enzyme 2 (ACE2) knockout (KO) hearts. Echocardiographic assessment of heart function showing M-mode images (**A**) and tissue Doppler imaging (**B**) showing marked reversal of the systolic dysfunction with persistent diastolic dysfunction in Akita/ACE2KO hearts treated with irbesartan. Quantification of echocardiographic data showing normalization of the reduction in left ventricular (LV) fractional shortening (LVFS) (**C**) and LV ejection fraction (LVEF) (**D**) in response to treatment with irbesartan, whereas the E/E′ ratio (**E**) was unaffected in Akita/ACE2KO mice. Myocardial oxidative stress as assessed by NADPH oxidase activity (**F**) and superoxide level-based dihydroethidium (DHE) fluorescence (**G**) showed a complete suppression of the elevated oxidative stress in Akita/ACE2KO hearts in response to AT1 receptor blockade. Western blot analysis showed restored phosphorylation of Akt (**H**) and elevated phosphorylation of eNOS (**I**) in response to treatment with irbesartan in Akita/ACE2KO hearts. AU, arbitrary unit; RR, relative ratio; Irb, irbesartan. n=12 for each group except for Akita/ACE2KO plus irbesartan group in which n=10, and (**H**) and (**I**) in which n=5. $P<0.05$ compared to all other groups.

verified by using the specific NADPH oxidase inhibitor, gp91phox ds tat peptide.

Adverse remodeling of the ECM is a key pathogenic factor in systolic heart failure and has been linked to activation of the RAS and NADPH oxidase.[7,8,36] Fluorescence-based imaging of the ECM showed a marked degradation of the ECM network and loss of collagen content in Akita/ACE2KO

hearts, whereas the WT, Akita, and ACE2KO hearts all showed an intact ECM (Figure 4E, F). Ang II–mediated oxidative stress is known to activate matrix metalloproteinases (MMPs), leading to degradation of ECM proteins. Gelatin zymography showed increased MMP9 level in Akita/ACE2KO hearts (Figure 5A, B). Importantly, loss of ACE2 increased pro-MMP2 and active MMP2 in Akita hearts

(Figure 5A, C). MMP2 and MMP9 are major gelatinases, whereas MMP2 also is a potent collagenase in the heart.[37] Gelatinase and collagenase activities were increased only in the Akita/ACE2KO hearts, thereby providing further evidence for an ECM-degrading environment in Akita/ACE2KO hearts (Figure 5D). Expression analysis of mRNA levels showed increased MMP9, MMP12, MMP13, and MMP14 (MT1-MMP) levels (Figure 5E–H) and MMP8 level (Online Figure VA), whereas MMP2 level was unchanged (Figure 5I), suggesting posttranscriptional activation of MMP2 is a key factor in mediating increased MMP2 protein levels. Although TIMP1 expression was increased in Akita/ACE2KO hearts, TIMP2 and TIMP3 levels were unchanged and TIMP4 level was reduced (Online Figure VB–E).

Loss of ACE2 Impairs Flow-Mediated Vasodilation and Increases Vascular Oxidative Stress in Akita Model: Role of the AT1 Receptor

Endothelial dysfunction and vascular oxidative stress have been linked to the development of diabetic cardiomyopathy.[25,38–40] Given the systemic disturbance of the RAS, we assessed the in vivo endothelial function in the Akita diabetic model and in response to ACE2 deficiency. We measured changes in blood flow velocity before and after ischemia-reperfusion of the femoral artery using high-resolution vascular ultrasonography. Baseline flow velocity was not different among the four experimental groups. Transient ischemia was followed by reactive hyperemia seen as an increase in flow velocity immediately after reperfusion in WT, Akita, ACE2KO, and Akita/ACE2KO mice (Figure 6A, B). Femoral flow velocity progressively declined to baseline value within 5 minutes in all groups, except in the Akita/ACE2KO mice, in which the flow velocity remained elevated even after 5 minutes of reperfusion (Figure 6A, B). These data show that in vivo flow-mediated dilation (FMD) is impaired in the Akita/ACE2KO model, suggestive of endothelial dysfunction. Increased vascular oxidative stress has been linked to endothelial dysfunction, a key mediator of FMD. Consistent with impaired FMD, aortic NADPH oxidase activity (Figure 6C) and DHE staining for superoxide (Figure 6D) showed increased oxidative stress in Akita/ACE2KO aorta and greater formation of nitrotyrosine (Figure 6E). We showed that loss of ACE2 leads to increased Ang II levels, a key mediator of vascular oxidative stress. We examined the impact of AT1 receptor blockade on the FMD and vascular oxidative stress. Treatment with the AT1 receptor blocker, irbesartan, prevented the impairment in FMD in Akita/ACE2KO mice based on femoral artery flow profile (Figure 7A, B), whereas the elevated NADPH oxidase was normalized (Figure 7C). DHE and nitrotyrosine fluorescence staining showed a marked reduction in superoxide levels and nitrotyrosine formation in response to AT1 receptor blockade, respectively (Figure 7D, E). These results show that loss of ACE2 impairs FMD and is linked to activation of the vascular NADPH oxidase system and formation of nitrotyrosine.

AT1 Receptor Blockade Prevents Systolic Dysfunction in the Akita/ACE2KO Model

Given the rescue of the vascular changes by AT1 receptor blockade, we next tested the critical role of the Ang II/AT1R

axis in mediating cardiac dysfunction in the Akita/ACE2KO murine model. Western blotting analysis showed significant increase of AT1R in Akita and Akita/ACE2KO hearts (Online Figure VIA). The increased AT1R density coupled with increased agonist stimulation likely perpetuate the Ang II–mediated adverse myocardial effects. Systolic dysfunction and the mild LV dilation in the Akita/ACE2KO mice showed a drastic normalization in response to treatment with irbesartan, whereas diastolic dysfunction persisted (Figure 8A–E, Online Table III), suggesting that the diastolic dysfunction is independent of the Ang II/AT1R axis. Irbesartan failed to prevent the diastolic dysfunction and elevated oxidative stress in Akita hearts (Online Figure VIB–I). In the Akita/ACE2KO mice, AT1R blockade significantly reduced the elevation in myocardial NADPH oxidase activity (Figure 8F) and superoxide generation (Figure 8G) while preventing the loss in phospho-Akt (Figure 8H) and restoring the elevation in phospho-eNOS levels (Figure 8I). The increased collagenase and gelatinase activity were also suppressed by irbesartan, resulting in normalization of the ECM architecture and collagen content in Akita/ACE2KO hearts (Online Figure VII). Although treatment with irbesartan and Ang 1–7 produced similar decrease in systolic blood pressure, Ang 1–7 failed to rescue the systolic dysfunction in Akita/ACE2KO mice (Online Figure VIII). These results show that we can uncouple systolic and diastolic dysfunction in a diabetic heart and pharmacological antagonism of the AT1 receptor reverses the systolic dysfunction and key pathophysiological processes in the Akita/ACE2KO hearts.

Discussion

Diabetic cardiomyopathy is characterized by early diastolic and vascular dysfunction, which progresses into systolic dysfunction, resulting in heart failure.[1–5] The RAS plays a central role in diabetic cardiomyopathy, and pharmacological inhibitors of the RAS are cornerstone to minimizing the cardiovascular complications. In an effort to determine the role of ACE2, we created ACE2-deficient Akita mice to determine the role of ACE2 in diabetic cardiomyopathy. The Akita murine model is a well-validated model of human diabetes[16,22] and also displays features compatible with type 2 diabetes, including insulin resistance.[23] Our study defines a critical role of ACE2 in suppressing the activation of the RAS in the heart such that loss of ACE2 results in increased Ang II/AT1 receptor signaling, adverse myocardial remodeling resulting in systolic dysfunction, vascular oxidative stress, and impaired flow-mediated dilation. In addition to its effects on the heart, Ang II affects virtually all vascular cells and is critical in endothelial dysfunction, which is a key determinant in the development and progression of diabetic complications.[4,25] Blockade of the AT1 receptor resulted in marked improvement in systolic dysfunction with reversal of the pathological effects in the vasculature and heart of Akita/ACE2KO mice. The failure of AT1 receptor blockade to reverse the diastolic dysfunction in the Akita model is consistent with clinical trials in patients with diastolic heart failure in which AT1 receptor blockers failed to improve clinical outcomes.[41,42]

The upregulation of ACE2 in diabetic Akita and db/db hearts is likely a key compensatory mechanism responsible for inhibiting activation of the RAS. In the diabetic condition, Ang II responses in myocardium and vasculature are augmented because of upregulation of Ang II type 1 receptor, thereby increasing Ang II sensitivity.[43] Inhibition of the AT1 receptor reduces adverse outcomes from heart failure in patients with diabetes.[9] ACE2, a homologue of ACE, is a carboxypeptidase that metabolizes Ang II to yield Ang 1–7 and lowers Ang II/Ang 1–7 ratio. The results from this study are consistent with other models of heart failure whereby loss of ACE2 exacerbates heart disease after myocardial infarction[12] and pressure overload.[14] Loss of ACE2 also exacerbates diabetic nephropathy,[44] which is a known correlate of cardiovascular disease.[45] Although loss of ACE2 elevated Ang II levels as predicted, we did not observe a corresponding decrease in Ang 1–7 levels in our model. Moreover, Ang 1–7 supplementation failed to rescue the systolic dysfunction in the Akita/ACE2KO mice. These results suggest that alternative pathways for Ang 1–7 generation are activated in a diabetic state such as the potent and high-capacity neprilysin enzyme and/or prolyl carboxypeptidase.[46–49]

Altered signaling may be an important driver of the phenotypic changes observed in the Akita and Akita/ACE2KO hearts. Because PKC has been shown to inhibit myofibrillar ATPase and sarcoplasmic reticular Ca^{2+} pump[26,50] activities, it is possible that upregulation of PKCα in the diabetic heart may have exacerbated the cardiomyopathy in the Akita/ACE2KO model. Akita hearts also show suppressed insulin-dependent signaling and evidence of lipotoxicity coupled with increased expression of pyruvate dehydrogenase kinase-4 and downregulation of SERCA2a. Akt and eNOS are positive modulators of myocardial contractility,[29,51] and the greater loss of phospho-Akt and phospho-eNOS in the Akita/ACE2KO hearts may contribute to the impaired systolic performance. Adverse remodeling of the ECM is a key pathogenic factor in heart failure and has been linked to activation of the RAS and NADPH oxidase.[7,8,36] Lack of myocardial fibrosis in Akita/ACEKO mice was accompanied by upregulation of MMP8, MMP9, MMP12, MMP13, and MMP14 expression, MMP2 and MMP9 protein levels (and their activities), which are the key ECM-degrading enzymes,[37,52] leading to further adverse remodeling of the ECM, LV dilation, and systolic dysfunction.[37,52]

Microvascular complications associated with diabetes also can adversely affect myocardial remodeling, and diabetic cardiomyopathy has been identified as a microvascular complication.[53,54] FMD is elicited by changes in blood flow, causing shear stress–induced release of nitric oxide by the endothelium.[55–58] Cellular oxidative stress and endothelial dysfunction are pivotal in the pathogenesis of cardiovascular diseases and are closely linked to circulating and tissue levels of Ang II.[59] Ang II can increase tyrosine-657 phosphorylation of eNOS, leading to decrease nitric oxide production and endothelial dysfunction.[60] Ang II–mediated reactive oxygen species production has the potential to further impair nitric oxide bioavailability by the consumption of nitric oxide and formation of peroxynitrite, leading to impaired endothelial relaxation and dysfunction.[39,58,61] Nitrotyrosine level, a marker of peroxynitrite formation, was elevated in Akita/ACE2KO aorta, which was reversed by treatment with irbesartan. AT1 receptor blockade clearly improved vascular oxidative stress, restored FMD, and prevented the development of systolic dysfunction in the Akita/ACE2KO model. Ang II activation of the AT1 receptor results in increased NADPH oxidase activity and enhanced reactive oxygen species generation.[34] The pathophysiological effects attributable to elevated Ang II levels in an ACE2-null environment are likely to be augmented by upregulation of the Ang II type 1 receptor in the Akita/ACE2KO hearts.

In summary, our study demonstrates loss of ACE2 exacerbates an underlying diabetic cardiomyopathy dysfunction resulting in a phenotype showing both diastolic and systolic dysfunction. We have identified increased oxidative stress, excessive ECM degradation, and vascular dysfunction brought about by upregulation of RAS in the absence of ACE2 as the underlying mechanism for the observed systolic dysfunction. Importantly, we have uncoupled diastolic and systolic dysfunction in our experimental models and have provided distinct mechanisms for each phenotype. Increased ACE2 expression and/or activity can represent a viable approach to minimize diabetes-induced cardiovascular complications.

Disclosures
None.

References

1. Kannel WB, Hjortland M, Castelli WP. Role of diabetes in congestive heart failure: The Framingham study. *Am J Cardiol*. 1974;34:29–34.
2. Grundy SM, Benjamin IJ, Burke GL, Chait A, Eckel RH, Howard BV, Mitch W, Smith SC Jr, Sowers JR. Diabetes and cardiovascular disease: A statement for healthcare professionals from the American Heart Association. *Circulation*. 1999;100:1134–1146.
3. Zimmet P, Alberti KG, Shaw J. Global and societal implications of the diabetes epidemic. *Nature*. 2001;414:782–787.
4. Boudina S, Abel ED. Diabetic cardiomyopathy revisited. *Circulation*. 2007;115:3213–3223.
5. From AM, Scott CG, Chen HH. The development of heart failure in patients with diabetes mellitus and pre-clinical diastolic dysfunction a population-based study. *J Am Coll Cardiol*. 2010;55:300–305.
6. Poornima IG, Parikh P, Shannon RP. Diabetic cardiomyopathy: The search for a unifying hypothesis. *Circ Res*. 2006;98:596–605.
7. Falcao-Pires I, Hamdani N, Borbely A, Gavina C, Schalkwijk CG, van der Velden J, van Heerebeek L, Stienen GJ, Niessen HW, Leite-Moreira AF, Paulus WJ. Diabetes mellitus worsens diastolic left ventricular dys-

function in aortic stenosis through altered myocardial structure and cardiomyocyte stiffness. *Circulation*. 2011;124:1151–1159.

8. Frustaci A, Kajstura J, Chimenti C, Jakoniuk I, Leri A, Maseri A, Nadal-Ginard B, Anversa P. Myocardial cell death in human diabetes. *Circ Res*. 2000;87:1123–1132.

9. Brenner BM, Cooper ME, de Zeeuw D, Keane WF, Mitch WE, Parving HH, Remuzzi G, Snapinn SM, Zhang Z, Shahinfar S, RENAAL Study Investigators. Effects of losartan on renal and cardiovascular outcomes in patients with type 2 diabetes and nephropathy. *N Engl J Med*. 2001;345:861–869.

10. Giacchetti G, Sechi LA, Rilli S, Carey RM. The renin-angiotensin-aldosterone system, glucose metabolism and diabetes. *Trends Endocrinol Metab*. 2005;16:120–126.

11. Carr AA, Kowey PR, Devereux RB, Brenner BM, Dahlof B, Ibsen H, Lindholm LH, Lyle PA, Snapinn SM, Zhang Z, Edelman JM, Shahinfar S. Hospitalizations for new heart failure among subjects with diabetes mellitus in the RENAAL and LIFE studies. *Am J Cardiol*. 2005;96:1530–1536.

12. Kassiri Z, Zhong J, Guo D, Basu R, Wang X, Liu PP, Scholey JW, Penninger JM, Oudit GY. Loss of angiotensin-converting enzyme 2 accelerates maladaptive left ventricular remodeling in response to myocardial infarction. *Circ Heart Fail*. 2009;2:446–455.

13. Zhong J, Basu R, Guo D, Chow FL, Byrns S, Schuster M, Loibner H, Wang XH, Penninger JM, Kassiri Z, Oudit GY. Angiotensin-converting enzyme 2 suppresses pathological hypertrophy, myocardial fibrosis and cardiac dysfunction. *Circulation*. 2010;122:717–728, 18 p following 728.

14. Bodiga S, Zhong JC, Wang W, Basu R, Lo J, Liu GC, Guo D, Holland SM, Scholey JW, Penninger JM, Kassiri Z, Oudit GY. Enhanced susceptibility to biomechanical stress in ACE2 null mice is prevented by loss of the p47phox NADPH oxidase subunit. *Cardiovasc Res*. 2011;91:151–161.

15. Wang W, Bodiga S, Das SK, Lo J, Patel V, Oudit GY. Role of ACE2 in diastolic and systolic heart failure. *Heart Fail Rev*. 2011 Jun 3 [Epub ahead of print].

16. Basu R, Oudit GY, Wang X, Zhang L, Ussher JR, Lopaschuk GD, Kassiri Z. Type 1 diabetic cardiomyopathy in the Akita (Ins2wt/C96Y) mouse model is characterized by lipotoxicity and diastolic dysfunction with preserved systolic function. *Am J Physiol Heart Circ Physiol*. 2009;297:H2096–H2108.

17. Heiss C, Sievers RE, Amabile N, Momma TY, Chen Q, Natarajan S, Yeghiazarians Y, Springer ML. In vivo measurement of flow-mediated vasodilation in living rats using high-resolution ultrasound. *Am J Physiol Heart Circ Physiol*. 2008;294:H1086–H1093.

18. Guo D, Kassiri Z, Basu R, Chow FL, Kandalam V, Damilano F, Liang W, Izumo S, Hirsch E, Penninger JM, Backx PH, Oudit GY. Loss of PI3K{gamma} enhances camp-dependent MMP remodeling of the myocardial N-cadherin adhesion complexes and extracellular matrix in response to early biomechanical stress. *Circ Res*. 2010;107:1275–1289.

19. Kandalam V, Basu R, Abraham T, Wang X, Soloway PD, Jaworski DM, Oudit GY, Kassiri Z. TIMP2 deficiency accelerates adverse post-myocardial infarction remodeling because of enhanced MT1-MMP activity despite lack of MMP2 activation. *Circ Res*. 2010;106:796–808.

20. Kandalam V, Basu R, Abraham T, Wang X, Awad A, Wang W, Lopaschuk GD, Maeda N, Oudit GY, Kassiri Z. Early activation of matrix metalloproteinases underlies the exacerbated systolic and diastolic dysfunction in mice lacking TIMP3 following myocardial infarction. *Am J Physiol Heart Circ Physiol*. 2010;299:H1012–H1023.

21. Mehta PK, Griendling KK. Angiotensin II cell signaling: Physiological and pathological effects in the cardiovascular system. *Am J Physiol Cell Physiol*. 2007;292:C82–C97.

22. Kakoki M, Takahashi N, Jennette JC, Smithies O. Diabetic nephropathy is markedly enhanced in mice lacking the bradykinin B2 receptor. *Proc Natl Acad Sci U S A*. 2004;101:13302–13305.

23. Hong EG, Jung DY, Ko HJ, Zhang Z, Ma Z, Jun JY, Kim JH, Sumner AD, Vary TC, Gardner TW, Bronson SK, Kim JK. Nonobese, insulin-deficient Ins2akita mice develop type 2 diabetes phenotypes including insulin resistance and cardiac remodeling. *Am J Physiol Endocrinol Metab*. 2007;293:E1687–E1696.

24. Ishii H, Koya D, King GL. Protein kinase c activation and its role in the development of vascular complications in diabetes mellitus. *J Mol Med (Berl)*. 1998;76:21–31.

25. Brownlee M. Biochemistry and molecular cell biology of diabetic complications. *Nature*. 2001;414:813–820.

26. Geraldes P, King GL. Activation of protein kinase c isoforms and its impact on diabetic complications. *Circ Res*. 106:1319–1331.

27. Bertrand L, Horman S, Beauloye C, Vanoverschelde JL. Insulin signalling in the heart. *Cardiovasc Res*. 2008;79:238–248.

28. Oudit GY, Penninger JM. Cardiac regulation by phosphoinositide 3-kinases and PTEN. *Cardiovasc Res*. 2009;82:250–260.

29. Sartoretto JL, Kalwa H, Pluth MD, Lippard SJ, Michel T. Hydrogen peroxide differentially modulates cardiac myocyte nitric oxide synthesis. *Proc Natl Acad Sci U S A*. 2011;108:15792–15797.

30. Majer M, Popov KM, Harris RA, Bogardus C, Prochazka M. Insulin downregulates pyruvate dehydrogenase kinase (PDK) mRNA: Potential mechanism contributing to increased lipid oxidation in insulin-resistant subjects. *Mol Genet Metab*. 1998;65:181–186.

31. Flagg TP, Cazorla O, Remedi MS, Haim TE, Tones MA, Bahinski A, Numann RE, Kovacs A, Schaffer JE, Nichols CG, Nerbonne JM. Ca2+-independent alterations in diastolic sarcomere length and relaxation kinetics in a mouse model of lipotoxic diabetic cardiomyopathy. *Circ Res*. 2009;104:95–103.

32. Schmidt U, del Monte F, Miyamoto MI, Matsui T, Gwathmey JK, Rosenzweig A, Hajjar RJ. Restoration of diastolic function in senescent rat hearts through adenoviral gene transfer of sarcoplasmic reticulum Ca(2+)-ATPase. *Circulation*. 2000;101:790–796.

33. Trost SU, Belke DD, Bluhm WF, Meyer M, Swanson E, Dillmann WH. Overexpression of the sarcoplasmic reticulum Ca(2+)-ATPase improves myocardial contractility in diabetic cardiomyopathy. *Diabetes*. 2002;51:1166–1171.

34. Privratsky JR, Wold LE, Sowers JR, Quinn MT, Ren J. AT1 blockade prevents glucose-induced cardiac dysfunction in ventricular myocytes: Role of the AT1 receptor and NADPH oxidase. *Hypertension*. 2003;42:206–212.

35. Griendling KK, FitzGerald GA. Oxidative stress and cardiovascular injury: Part II: Animal and human studies. *Circulation*. 2003;108:2034–2040.

36. Neumann S, Huse K, Semrau R, Diegeler A, Gebhardt R, Buniatian GH, Scholz GH. Aldosterone and D-glucose stimulate the proliferation of human cardiac myofibroblasts in vitro. *Hypertension*. 2002;39:756–760.

37. Spinale FG. Myocardial matrix remodeling and the matrix metalloproteinases: Influence on cardiac form and function. *Physiol Rev*. 2007;87:1285–1342.

38. Sheetz MJ, King GL. Molecular understanding of hyperglycemia's adverse effects for diabetic complications. *JAMA*. 2002;288:2579–2588.

39. Xu J, Zou MH. Molecular insights and therapeutic targets for diabetic endothelial dysfunction. *Circulation*. 2009;120:1266–1286.

40. Shivu GN, Phan TT, Abozguia K, Ahmed I, Wagenmakers A, Henning A, Narendran P, Stevens M, Frenneaux M. Relationship between coronary microvascular dysfunction and cardiac energetics impairment in type 1 diabetes mellitus. *Circulation*. 2010;121:1209–1215.

41. Massie BM, Carson PE, McMurray JJ, Komajda M, McKelvie R, Zile MR, Anderson S, Donovan M, Iverson E, Staiger C, Ptaszynska A, I-PRESERVE Investigators. Irbesartan in patients with heart failure and preserved ejection fraction. *N Engl J Med*. 2008;359:2456–2467.

42. Paulus WJ, van Ballegoij JJ. Treatment of heart failure with normal ejection fraction: An inconvenient truth! *J Am Coll Cardiol*. 2010;55:526–537.

43. Sodhi CP, Kanwar YS, Sahai A. Hypoxia and high glucose upregulate at1 receptor expression and potentiate ANG II-induced proliferation in VSM cells. *Am J Physiol Heart Circ Physiol*. 2003;284:H846–H852.

44. Wong DW, Oudit GY, Reich H, Kassiri Z, Zhou J, Liu QC, Backx PH, Penninger JM, Herzenberg AM, Scholey JW. Loss of angiotensin-converting enzyme-2 (Ace2) accelerates diabetic kidney injury. *Am J Pathol*. 2007;171:438–451.

45. Gerstein HC, Mann JF, Yi Q, Zinman B, Dinneen SF, Hoogwerf B, Halle JP, Young J, Rashkow A, Joyce C, Nawaz S, Yusuf S, HOPE Study Investigators. Albuminuria and risk of cardiovascular events, death, and heart failure in diabetic and nondiabetic individuals. *JAMA*. 2001;286:421–426.

46. Allred AJ, Diz DI, Ferrario CM, Chappell MC. Pathways for angiotensin-(1–7) metabolism in pulmonary and renal tissues. *Am J Physiol Renal Physiol*. 2000;279:F841–F850.

47. Chappell MC, Allred AJ, Ferrario CM. Pathways of angiotensin-(1–7) metabolism in the kidney. *Nephrol Dial Transplant*. 2001;16 (Suppl 1):22–26.

48. Schmaier AH. The kallikrein-kinin and the renin-angiotensin systems have a multilayered interaction. *Am J Physiol Regul Integr Comp Physiol*. 2003;285:R1–R13.

49. Standeven KF, Hess K, Carter AM, Rice GI, Cordell PA, Balmforth AJ, Lu B, Scott DJ, Turner AJ, Hooper NM, Grant PJ. Neprilysin, obesity and the metabolic syndrome. *Int J Obes (Lond)*. 2011;35:1031–1040.

50. Noland TA Jr, Kuo JF. Protein kinase c phosphorylation of cardiac troponin i or troponin t inhibits Ca2(+)-stimulated actomyosin MgATPase activity. *J Biol Chem*. 1991;266:4974–4978.

51. Condorelli G, Drusco A, Stassi G, Bellacosa A, Roncarati R, Iaccarino G, Russo MA, Gu Y, Dalton N, Chung C, Latronico MV, Napoli C, Sadoshima J, Croce CM, Ross J Jr. Akt induces enhanced myocardial contractility and cell size in vivo in transgenic mice. *Proc Natl Acad Sci U S A*. 2002;99:12333–12338.

52. Moore L, Fan D, Basu R, Kandalam V, Kassiri Z. Tissue inhibitor of metalloproteinases (TIMPS) in heart failure. *Heart Fail Rev*. 2011 Jun 30 [Epub ahead of print].

53. Cheung N, Bluemke DA, Klein R, Sharrett AR, Islam FM, Cotch MF, Klein BE, Criqui MH, Wong TY. Retinal arteriolar narrowing and left ventricular remodeling: The multi-ethnic study of atherosclerosis. *J Am Coll Cardiol*. 2007;50:48–55.

54. Factor SM, Minase T, Sonnenblick EH. Clinical and morphological features of human hypertensive-diabetic cardiomyopathy. *Am Heart J*. 1980;99:446–458.

55. Furchgott RF, Zawadzki JV. The obligatory role of endothelial cells in the relaxation of arterial smooth muscle by acetylcholine. *Nature*. 1980;288:373–376.

56. Pohl U, Holtz J, Busse R, Bassenge E. Crucial role of endothelium in the vasodilator response to increased flow in vivo. *Hypertension*. 1986;8:37–44.

57. Cooke JP, Rossitch E Jr, Andon NA, Loscalzo J, Dzau VJ. Flow activates an endothelial potassium channel to release an endogenous nitrovaso-dilator. *J Clin Invest*. 1991;88:1663–1671.

58. Rajagopalan S, Kurz S, Munzel T, Tarpey M, Freeman BA, Griendling KK, Harrison DG. Angiotensin II-mediated hypertension in the rat increases vascular superoxide production via membrane NADH/NADPH oxidase activation. Contribution to alterations of vasomotor tone. *J Clin Invest*. 1996;97:1916–1923.

59. Dzau VJ. Theodore Cooper Lecture: Tissue angiotensin and pathobiology of vascular disease: A unifying hypothesis. *Hypertension*. 2001;37:1047–1052.

60. Loot AE, Schreiber JG, Fisslthaler B, Fleming I. Angiotensin ii impairs endothelial function via tyrosine phosphorylation of the endothelial nitric oxide synthase. *J Exp Med*. 2009;206:2889–2896.

61. Doughan AK, Harrison DG, Dikalov SI. Molecular mechanisms of angiotensin II-mediated mitochondrial dysfunction: Linking mitochondrial oxidative damage and vascular endothelial dysfunction. *Circ Res*. 2008;102:488–496.

Novelty and Significance

What Is Known?

- Diabetes mellitus results in severe cardiovascular complications, and heart disease remains the major cause of death in patients with diabetes.
- Activation of the rennin-angiotensin system (RAS) plays a key role in the progression of diabetic complications, and AT1 receptor blockers reduce these complications.
- Angiotensin-converting enzyme 2 (ACE2; a type I transmembrane protein that converts angiotensin (Ang) II into Ang 1–7) is a negative regulator of the RAS.

What New Information Does This Article Contribute?

- Loss of ACE2 in diabetic Akita mice exhibits exacerbated diabetic cardiomyopathy, resulting in systolic dysfunction associated with increased oxidative stress and extracellular matrix (ECM) degradation.
- Loss of ACE2 increased vascular oxidative stress and dysfunction in diabetic mice.
- Treatment with AT1 receptor blocker, irbesartan, prevented the systolic and vascular dysfunction in the Akita/ACE2KO model.

Diabetic cardiomyopathy is characterized by early diastolic and vascular dysfunction that progresses into systolic dysfunction, resulting in heart failure. The RAS has been shown to play an important role in diabetic cardiovascular complications. ACE2, a monocarboxypeptidase, metabolizes Ang II to yield Ang 1–7, essentially negatively regulating the RAS. Our study demonstrates that myocardial ACE2 levels are increased in Akita and db/db diabetic models. Loss of ACE2 exacerbates underlying diabetic cardiomyopathy characterized by diastolic dysfunction, resulting in a phenotype showing both diastolic dysfunction and systolic dysfunction, which were associated with increased oxidative stress and ECM degradation in Akita mice. Loss of ACE2 also enhanced diabetes-induced increase in vascular oxidative stress and vascular dysfunction. Treatment with the AT1R antagonist, irbesartan, rescued the systolic and vascular dysfunction in the ACE2-deficient Akita diabetic mice, as a result of decreased oxidative stress and ECM degradation. We conclude that increased ACE2 expression and/or activity may be a viable approach to minimize secondary cardiovascular complications of diabetes.
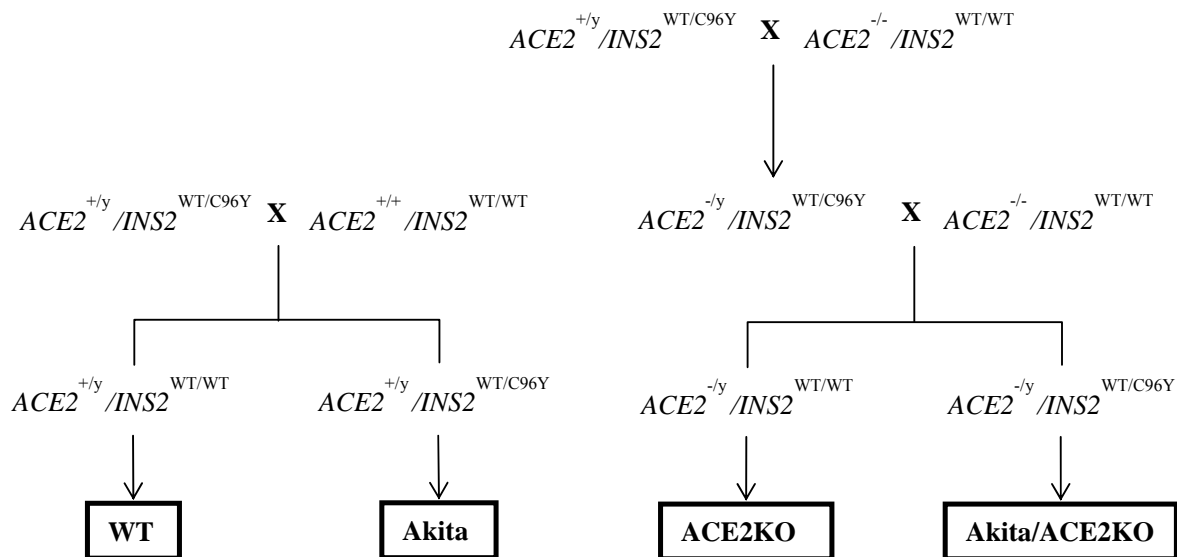
SUPPLEMENTAL MATERIAL

Loss of ACE2 exacerbates diabetic cardiovascular complications and leads to systolic and vascular dysfunction: a critical role of the Ang II/AT1 receptor axis

by

Vaibhav B. Patel PhD, Sreedhar Bodiga PhD, Ratnadeep Basu MD, Subhash K. Das, MSc, Wang Wang MSc, Zuocheng Wang PhD, Jennifer Lo BSc, Maria B. Grant MD, JiuChang Zhong MSc, MD, Zamaneh Kassiri PhD and Gavin Y. Oudit MD, PhD, FRCPC

Supplemental Methods

Breeding Scheme. We used the following breeding scheme to generate WT, Akita, ACE2KO and Akita/ACE2KO murine models used in this study.

$$ACE2^{+/y}/INS2^{WT/C96Y} \quad \mathbf{X} \quad ACE2^{-/-}/INS2^{WT/WT}$$

$$\downarrow$$

$$ACE2^{+/y}/INS2^{WT/C96Y} \quad \mathbf{X} \quad ACE2^{+/+}/INS2^{WT/WT} \qquad\qquad ACE2^{-/y}/INS2^{WT/C96Y} \quad \mathbf{X} \quad ACE2^{-/-}/INS2^{WT/WT}$$

$$ACE2^{+/y}/INS2^{WT/WT} \qquad ACE2^{+/y}/INS2^{WT/C96Y} \qquad ACE2^{-/y}/INS2^{WT/WT} \qquad ACE2^{-/y}/INS2^{WT/C96Y}$$

| WT | Akita | ACE2KO | Akita/ACE2KO |

Tail-Cuff Systolic Blood Pressure. For the measurement of tail-cuff systolic blood pressure (TC-SBP), conscious mice were placed in the restrainers and their body temperature was maintained at ~ 34 °C by the warming chamber. The IITC tail cuff sensor containing both the inflation cuff and the photoelectric sensor was placed on the tail and attached to the restrainer. The cuff was inflated to a pressure of 200 mmHg and then deflated slowly. Upon reappearance of pulse signals, TC-SBP data from the IITC amplifier was recorded, analyzed and reported by the IITC software (IITC Life Science Blood Pressure System, Woodland Hills, CA). The mice were trained on three occasions before actual

recordings were made and the corresponding TC-SBPs were averaged from three readings and used for the averaged comparisons.

Echocardiography and Tissue Doppler Imaging. Transthoracic echocardiography was performed and analyzed in a blinded manner as described previously using a Vevo 770 high-resolution imaging system equipped with a 30-MHz transducer (RMV-707B; VisualSonics, Toronto, Canada).[1, 2] Mice were anesthetized with 0.75% isoflurane for the duration of the recordings. M-mode images were obtained for measurements of LV wall thickness (LVWT), LV end-diastolic diameter (LVEDD) and LV end-systolic diameter (LVESD) (measures of LV dilation). LV fractional shortening (FS) was calculated as FS (%)=(LVEDD–LVESD)/LVEDD)x100 and LV ejection fraction (EF) (%)=(LVEDV-LDESV)/LVEDVx100 as measures of systolic function. Diastolic function was assessed using pulsed-wave Doppler imaging of the transmitral filling pattern with the early transmitral filling wave (E-wave) followed by the late filling wave due to atrial contraction (A-wave). Isovolumetric relaxation time (IVRT) was calculated as the time from closure of the aortic valve to initiation of the E-wave. The deceleration time (DT) of the E-wave was determined by measuring the time needed for the down-slope of the peak of the E-wave to reach the baseline while the rate of E-wave deceleration rate (EWDR) was calculated as the E-wave divided by the DT. Tissue Doppler imaging (TDI) was made at the mitral valve annulus in the modified four-chamber view at the base of the LV with the assessment of peak annular systolic (S'), early diastolic (E') and late diastolic (A') peak annular velocities.[3, 4] The TDI technique represents a novel and validated technique to assess systolic and diastolic function with reduction in E' and E'/A' ratio and elevation in E/E' being considered a valid marker of elevated LV filling pressure and diastolic dysfunction. [3, 4]

TaqMan Real-time PCR. RNA expression levels of various genes were determined by TaqMan real-time PCR as previously described (see Supplemental Table I for list of primers and probes).[5, 6] Total RNA was extracted from flash-frozen tissuesusing TRIzol, and cDNA was synthesized from 1 μg RNA by using a random hexamer. For each gene, a standard curve was generated using known concentrations of cDNA (0.625, 1.25, 2.5, 5, 10 and 20 μg) as a function of cycle threshold (CT). Expression analysis of the reported genes was performed by TaqMan real-time-PCR using ABI 7900 Sequence Detection System. The SDS2.2 software (integral to ABI7900 real-time machine) fits the CT values for the experimental samples and generates values for cDNA levels. All samples were run in triplicates in 384 well plates. 18S rRNA was used as an endogenous control.

Dihydroethidium Fluorescence. Dihydroethidium (DHE), an oxidative fluorescent dye, was used to measure superoxide (O_2^-) levels in heart tissues from ACE2KO and WT mice as previously described.[6] Briefly, the cultured and treated cardiomyocytes were washed with clear media (Eagle's MEM) and then incubated at 37 °C for 30 min with DHE (20 μM) in clear media. For heart samples, 20 μm fresh frozen tissue sections were washed with hanks balanced salt solution (HBSS) with magnesium and calcium and then incubated at 37 °C for 30 min with DHE (20 μM) in HBSS. For a separated experiment, heart tissue sections from mice with Ang II pumps or Ang II-treated cardiomyocytes were incubated with polyethylene glycol-conjugated superoxide dismutase (PEG-SOD) (500U/mL) at 37 °C for 30 min prior to 30-min exposure of DHE (20 μM). In addition, one cell plate or one tissue slide was kept without DHE for blank control. The cell plates or tissue slides were wrapped with foil to minimize them exposure to light. Fluorescent images were observed with an Olympus Fluoview laser-scanning confocal microscope mounted on an Olympus microscope selected with CY3 (red) channel.

Lucigenin-Enhanced Chemiluminescence. The activities of nicotinamide adenine dinucleotide phosphate (NADPH) oxidase in hearts of mice were quantified by lucigenin-enhanced chemiluminescence as previously described.[6, 7] Briefly, the cardiomyocytes and heart homogenates (200 μg total proteins) were collected in 100 μl of phosphate buffer solution (PBS) mixture with phosphatase inhibitor and protease inhibitor and then centrifuged at 1000 g for 10 min. The supernatants were then collected and added NADPH (1mM) and lucigenin (50 μM) for NADPH oxidase activities assay with FB-12 luminometer in the presence or absence of diphenylene iodonium

(DPI, 10 μM), a selective inhibitor of flavin-containing enzymes including NADPH oxidase. Data were calculated as the change in the rate of luminescence per minute per milligram of tissue.

Terminal deoxynucleotidyltransferase – mediated dUTP nick-end labeling (TUNEL): In situ DNA fragmentation was detected using the TUNEL assay kit (Invitrogen) according to manufacturer's instructions. Briefly, 15 μm thick LV cryosections were fixed with 4% paraformaldehyde and washed in Dulbecco's PBS. The sections were then permeabilized with 0.1% Triton X-100 in 0.1% sodium citrate and washed with wash buffer. After one hour incubation with DNA labeling solution (terminal deoxynucleotidyltransferase and BrdUTP in reaction buffer) the sections were treated with Alexa Fluor 488 conjugated mouse anti-BrdU and counterstained with propidium iodide. The sections were mounted using Prolong Gold antifade mounting medium and visualized under fluorescence microscope (Olympus IX 81). TUNEL positive cells were counted using 60X magnification images with MetaMorph (Basic version 7.7.0.0) software and magnitude of apoptosis was expressed as % apoptotic cells.

Histological Analysis. To study the heart morphometry, hearts were arrested in diastole with 1 M KCl, fixed with 10% buffered formalin, and embedded in paraffin. Ten micrometer thick sections were stained with Picro-sirius Red (PSR) and visualized under fluorescence microscope (Olympus IX81). PSR stained sections were used to assess interstitial and perivascular fibrosis. Five micrometer thick LV cryosections were stained with Oregon 488 conjugated wheat germ agglutinin (WGA) and counterstained with DAPI. The WGA-stained sections were visualized under fluorescence microscope (Olympus IX81) used to measure the myocyte cross-sectional area using Metamorph (Version 7.7.0.0) software.

Immunohistochemistry. Nitrotyrosine immunostaining was performed on 5 micrometer thick aorta cryosections. Briefly, OCT embedded aorta cryosections were fixed with 4% formaldehyde for 20 minutes, and rehydrated with PBS for 30 minutes. Aorta sections were then permeabilized with 0.2% Triton-X100 in PBS for 5 minutes, followed by blocking with 4% bovine serum albumin for 1 hour. They were then incubated with rabbit anti-nitrotyrosine (1:250; Millipore) overnight at 4°C in a humidified chamber. Sections were incubated with TRITC conjugated goat anti-rabbit (1:160; Abcam) secondary antibody at 37°C for 1 hour in a humidified chamber. Aorta sections were visualized under fluorescence microscope (IX81, Olympus) after mounting with ProlongGold antifade mounting medium with DAPI (Invitrogen). The cells were washed with PBS, three times for 5 minutes each, in between each steps.

Western Blot Analysis. The phosphorylated and/or total proteins fromheart tissues and aortae of mice were measured by Western blot analysis as previously described.[2, 6] Protein was extracted in 25 mM Tris, 62.5 mM NaCl, 1.25 mM PMSF, 62.5 mM Glycerol-2-phosphate, 12.5 mM sodium pyrophosphate, 125 μM NaF, 6.25 μg/ml leupeptine, 312.5 μM sodium orthovanadate, 12.5% glycerol, pH 7.4, supplemented with 5% sodium dodecyl sulphate (SDS) and 1% Triton X-100. After quantification using the BCA Protein Array Kit (Pierce, Rockford, IL, USA), protein samples were separated by 8%~12% SDS-polyacrylamide gel electrophoresis and then transferred to nitrocellulose membrane (Millipore). The membrane was blocked with 5% milk in Tris-Buffered Saline Tween-20 (TBST) for 2 h and then incubated overnight at 4°C with primary antibody against ACE2 (90 KD), PKCα (80 kDa), α-tubulin (55 kDa) and total and phosphorylated ERK1 (44 kDa), ERK2 (42 kDa), JAK2 (130 kDa) STAT3 (80 kDa) and phosphorylated and total eNOS (140 KDa) (Santa Cruz and Cell Signaling Inc.). The primary antibody was then removed, and membrane washed thoroughly with TBST. Membrane was then incubated with goat anti-rabbit IgG coupled to horseradish peroxidase (HRP) at a 1:3000 dilution in TBST for l h at room temperature, then rinsed thoroughly with TBST and then ECL was added. Blots were scanned and quantified using ImageQuant[TM]LAS 4000 (GE Healthcare, Biosciences, Quebec, Canada).

Supplemental References

1.   Basu R, Oudit GY, Wang X, Zhang L, Ussher JR, Lopaschuk GD, Kassiri Z. Type 1 diabetic cardiomyopathy in the akita (ins2wt/c96y) mouse model is characterized by lipotoxicity and diastolic dysfunction with preserved systolic function. *Am J Physiol Heart Circ Physiol*. 2009;297:H2096-2108.

2.   Zhong JC, Basu R, Guo D, Chow FL, Byrns S, Shuster M, Loibner H, Wang X, Penninger JM, Kassiri Z, Oudit GY. Angiotensin converting enzyme 2 suppresses pathological hypertrophy, myocardial fibrosis and cardiac dysfunction. *Circulation*. 2010;122:717-728.

3.   Schaefer A, Klein G, Brand B, Lippolt P, Drexler H, Meyer GP. Evaluation of left ventricular diastolic function by pulsed doppler tissue imaging in mice. *J Am Soc Echocardiogr*. 2003;16:1144-1149.

4.   Yu CM, Sanderson JE, Marwick TH, Oh JK. Tissue doppler imaging a new prognosticator for cardiovascular diseases. *J Am Coll Cardiol*. 2007;49:1903-1914.

5.   Kassiri Z, Oudit GY, Sanchez O, Dawood F, Mohammed FF, Nuttall RK, Edwards DR, Liu PP, Backx PH, Khokha R. Combination of tumor necrosis factor-alpha ablation and matrix metalloproteinase inhibition prevents heart failure after pressure overload in tissue inhibitor of metalloproteinase-3 knock-out mice. *Circ Res*. 2005;97:380-390.

6.   Kassiri Z, Zhong J, Guo D, Basu R, Wang X, Liu PP, Scholey JW, Penninger JM, Oudit GY. Loss of angiotensin-converting enzyme 2 accelerates maladaptive left ventricular remodeling in response to myocardial infarction. *Circ Heart Fail*. 2009;2:446-455.

7.   Oudit GY, Kassiri Z, Patel MP, Chappell M, Butany J, Backx PH, Tsushima RG, Scholey JW, Khokha R, Penninger JM. Angiotensin ii-mediated oxidative stress and inflammation mediate the age-dependent cardiomyopathy in ace2 null mice. *Cardiovasc Res*. 2007;75:29-39.

Supplemental Tables

Supplemental Table I. List of Taqman Primers and Probes.

Gene	Primers/Probes	Sequence (Primer: 5'-3'; Probe: 5'-FAM- -TAMRA-3')
α-SA	Forward Primer	CAGCCGGCGCCTGTT
	Reverse Primer	CCACAGGGCTTTGTTTGAAAA
	Probe	TTGACGTGTACATAGATTGACTCGTTTTACCTCATTTTG
β-MHC	Forward Primer	GTGCCAAGGGCCTGAATGAG
	Reverse Primer	GCAAAGGCTCCAGGTCTGA
	Probe	ATCTTGTGCTACCCAGCTCTAA
BNP	Forward Primer	CTGCTGGAGCTGATAAGAGA
	Reverse Primer	TGCCCAAAGCAGCTTGAGAT
	Probe	CTCAAGGCAGCACCCTCCGGG
MMP-2	Forward Primer	AACTACGATGATGACCGGAAGTG
	Reverse Primer	TGGCATGGCCGAACTCA
	Probe	TCTGTCCTGACCAAGGATATAGCCTATTCCTCG
MMP-9	Forward Primer	CGAACTTCGACACTGACAAGAAGT
	Reverse Primer	GCACGCTGGAATGATCTAAGC
	Probe	TCTGTCCAGACCAAGGGTACAGCCTGTTC
MMP-8	Forward Primer	GATTCAGAAGAAACGTGGACTCAA
	Reverse Primer	CATCAAGGCACCAGGATCAGT
	Probe	CATGAATTTGGACATTCTTTGGGACTCTCTCAC
MMP-12	Forward Primer	GAAACCCCCATCCTTGACAA
	Reverse Primer	TTCCACCAGAAGAACCAGTCTTTAA
	Probe	AGTCCACCATCAACTTTCTGTCACCAAAGC
MMP-13	Forward Primer	GGGCTCTGAATGGTTATGACATTC
	Reverse Primer	AGCGCTCAGTCTCTTCACCTCTT
	Probe	AAGGTTATCCCAGAAAAATATCTGACCTGGGATTC
MMP-14	Forward Primer	AGGAGACAGAGGTGATCATCATTG
	Reverse Primer	GTCCCATGGCGTCTGAAGA
	Probe	CCTGCCGGTACTACTGCTGCTCCTG
TIMP-1	Forward Primer	CATGGAAAGCCTCTGTGGATATG
	Reverse Primer	AAGCTGCAGGCACTGATGTG
	Probe	CTCATCACGGGCCGCCTAAGGAAC
TIMP-2	Forward Primer	CCAGAAGAAGAGCCTGAACCA
	Reverse Primer	GTCCATCCAGAGGCACTCATC
	Probe	ACTCGCTGTCCCATGATCCCTTGC
TIMP-3	Forward Primer	CCG CAG CGG ACC ACA AC
	Reverse Primer (427)	CCG GAT CAC GAT GTC GGA
	Reverse Primer (423)	GGA TCA CGA TGT CGG AGT TGC
	Probe	CTA CCA TGA CTC CCT GGC TT
TIMP-4	Forward Primer	TGCAGAGGGAGAGCCTGAA
	Reverse Primer	GGTACATGGCACTGCATAGCA
	Probe	CCACCAGAACTGTGGCTGCCAAATC

5

Supplemental Table II. Echocardiographic Data in WT, Akita, ACE2KO and Akita/ACE2KO mice at 6 months of age.

Parameter	WT	Akita	ACE2KO	Akita/ACE2KO
N	10	10	10	12
HR (bpm)	489±16	474±13	478±12	485±14
E-wave (mm/s)	685±24.8	702±31.6	656±41	691±33.9
A-wave (mm/s)	445±47.3	441±40	438±27	301±23.6
E/A Ratio	1.54±0.1	1.59±0.09	1.5±0.06	2.29±0.12[†]
IVRT (ms)	15.8±0.66	18.7±0.94*	16.4±0.78	13.4±0.96*
E′ (mm/s)	26.3±1.7	21.8±1.86	28.1±1.6	20.3±2.5*
E/E′ Ratio	27.9±1.8	33.1±1.7*	24.1±2.5	34±2.8*
A′	24.4±1.4	29.2±1.5*	25.1±1.2	31.2±2.5*
E′/A′	1.14±0.06	0.74±0.07*	1.12±0.05	0.65±0.08*
LA Size (mm)	1.85±0.07	2.17±0.05*	1.79±0.09	2.39±0.11*,[†]
LVEDD (mm)	3.79±0.05	3.71±0.04	3.77±0.06	3.86±0.08
LVESD (mm)	2.59±0.06	2.52±0.05	2.54±0.06	2.89±0.12
LVFS (%)	31.6±2.1	32.1±1.9	32.6±1.8	25.1±2.2[†]
LVEF (%)	62.7±2.4	60.4±2	63.1±1.69	49.9±2.53[†]
VCFc (circ/s)*10	6.3±0.51	6.13±0.38	6.22±0.41	4.71±0.3[†]
LVPWT (mm)	0.66±0.03	0.71±0.023	0.69±0.02	0.67±0.024

HR=heart rate; E-wave=peak early transmitral inflow mitral E velocity; A-wave=transmitral inflow velocity due to atrial contraction; IVRT=isovolumetric relaxation time; DT=deceleration time; EWDR=E-wave deceleration rate (E-wave/DT); E′=early diastolic tissue Doppler velocity; LVEDD=left ventricular end diastolic diameter; LVESD=left ventricular end systolic diameter; LVFS=LV fractional shortening; LVEF=LV ejection fraction; VCFc=Velocity of Circumferential Shortening corrected for Heart Rate; LVPWT=LV Posterior Wall Thickness. Results are presented as mean±S.E.M. *$p<0.05$ for the main effects and [†]$p<0.05$ for the interaction using two-way ANOVA.

Supplemental Table III. Echocardiographic assessment of diastolic and systolic function in Akita/ACE2KO mice in response to AT1 receptor blockade at 6 months of age.

Parameter	WT	Akita/ACE2KO +Placebo	Akita/ACE2KO +Irbesartan
N	12	12	10
E′ (mm/s)	26.3±1.7*	20.3±2.5	20.9±1.2
E/E′ Ratio	27.9±1.8*	34±2.8	33.8±2
E′/A′	1.14±0.06*	0.65±0.08	0.83±0.07
LA Size (mm)	1.85±0.07*	2.39±0.11	2.47±0.04
LVFS (%)	31.6±2.1*	25.1±2.2	28.6±1.42
LVEF (%)	62.7±2.4*	49.9±2.53	58.7±2.1
VCFc (circ/s)*10	6.3±0.51*	4.71±0.3	5.51±0.2

see supplemental Table II for abbreviations. Results are presented as mean±S.E.M. *p<0.05 compared to all other groups.
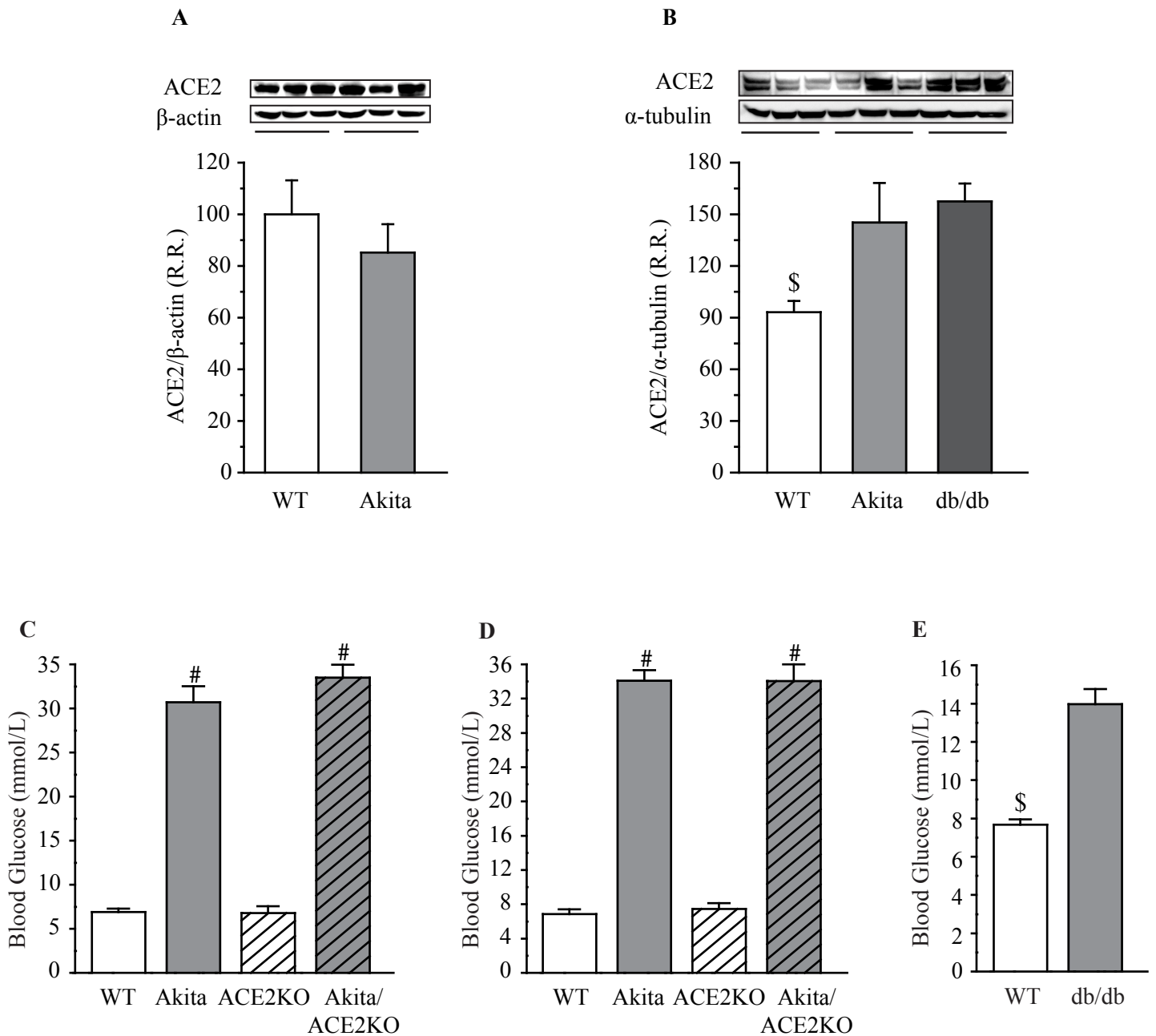
Supplemental Figure I. Western blot analysis showing no detectable changes in ACE2 expression in 6 months old Akita kidneys (A) while ACE2 levels were increased to comparable levels in 6 months old Akita and db/db mice hearts (B) (n=5). Sustained hyperglycemia in Akita and Akita/ACE2KO mice based on random blood glucose at 3 months (C) and 6 months (D) while 6 months old db/db mice also showed hyperglycemia based on random blood glucose levels (E) (n=8). R.R.=Relative Ratio. $p<0.05 compared to all other groups; #p<0.05 for the interaction using two-way ANOVA.
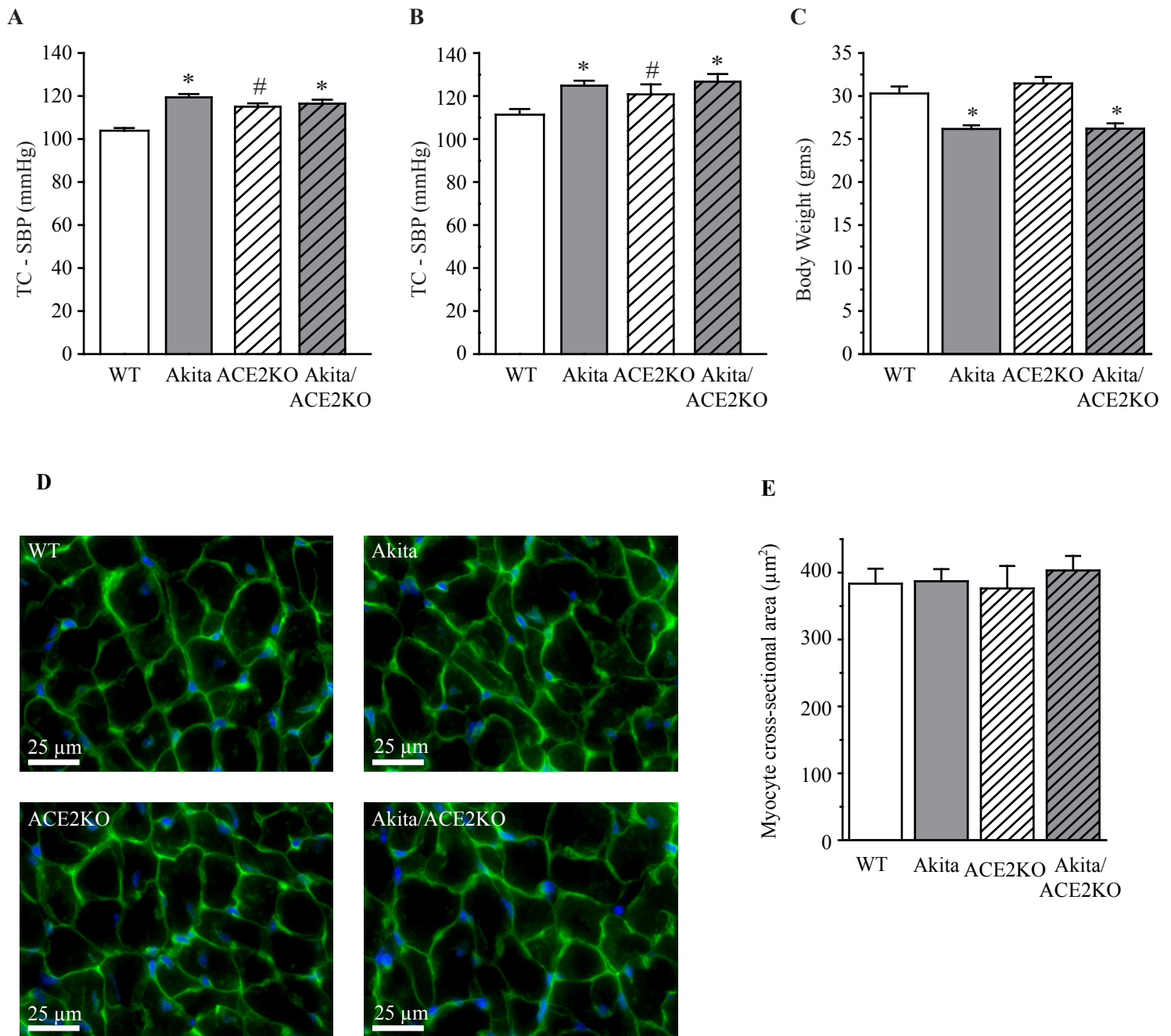
Supplemental Figure II. Akita mice showed a mild hypertension based on tail-cuff systolic blood pressure (TC-SBP) measurements at 3 months (A) and 6 months (B) while Akita and Akita/ACE2KO mice showed a small decrease in body weight at 6 months of age (C) (n=10). No overt hypertrophy was observed in any heart as assessed by wheat germ agglutinin (WGA) staining (D) with morphometric analysis of WGA staining showing no difference in myocyte cross-sectional area (E) (n=5). *p<0.05 for the main effects and #p<0.05 for the interaction using two-way ANOVA.
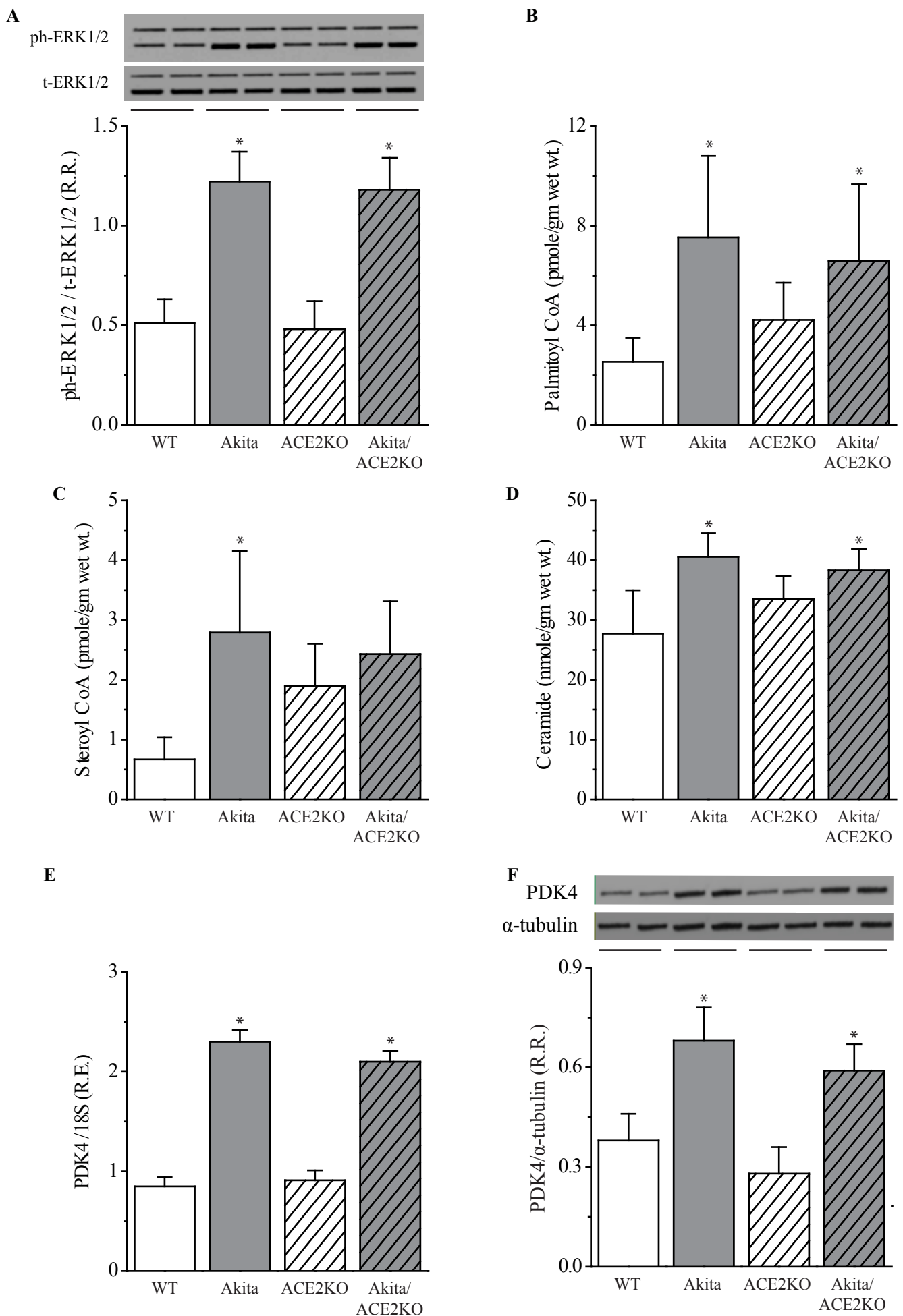
Supplemental Figure III. Western blot analysis of phospho (threonine-177) and total extracellular signal-regulated kinases 1/2 (ERK 1/2) showed equivalent elevation in ERK 1/2 phosphorylation in Akita and Akita/ACE2KO hearts (A). Equivalent lipotoxicity in Akita and Akita/ACE2KO hearts, as assessed by myocardial levels of long-chain fatty acids, palmitoyl coA (B), steroyl coA (C) and ceramide levels (D) and mRNA expression of PDK4 (E) and protein (F) levels showing similar increase in Akita and Akita/ACE2KO hearts. n=8 per group except for A and F where n=5. PDK4=pyruvate dehydrogenase kinase 4. *p<0.05 for the main effects using two-way ANOVA.
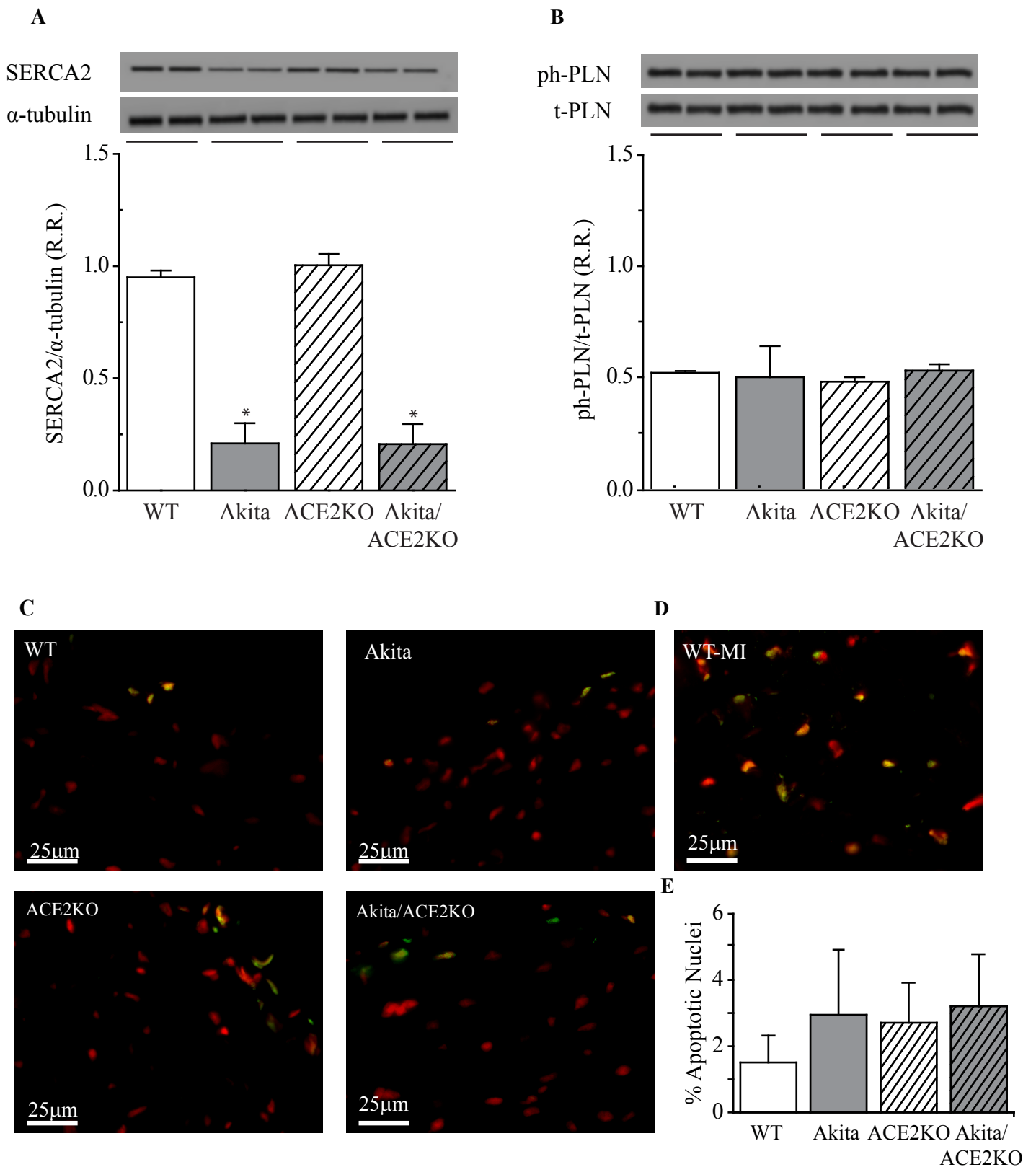
Supplemental Figure IV. Western blot analysis of SERCA2a (A) and phospho (serine-16) and total phospholamban (B) showing reduced SERCA2 levels in Akita and Akita/ACE2KO hearts. TUNEL assay based on fluorescence staining of apoptotic nuclei (C) with a positive control from a post-myocardial infarction LV sample (D) and quantification of the percent of apoptotic nuclei (E) showing a lack of an increase in apoptosis. R.R.=Relative Ratio; n=5 per group. *$p < 0.05$ for the main effects using two-way ANOVA.
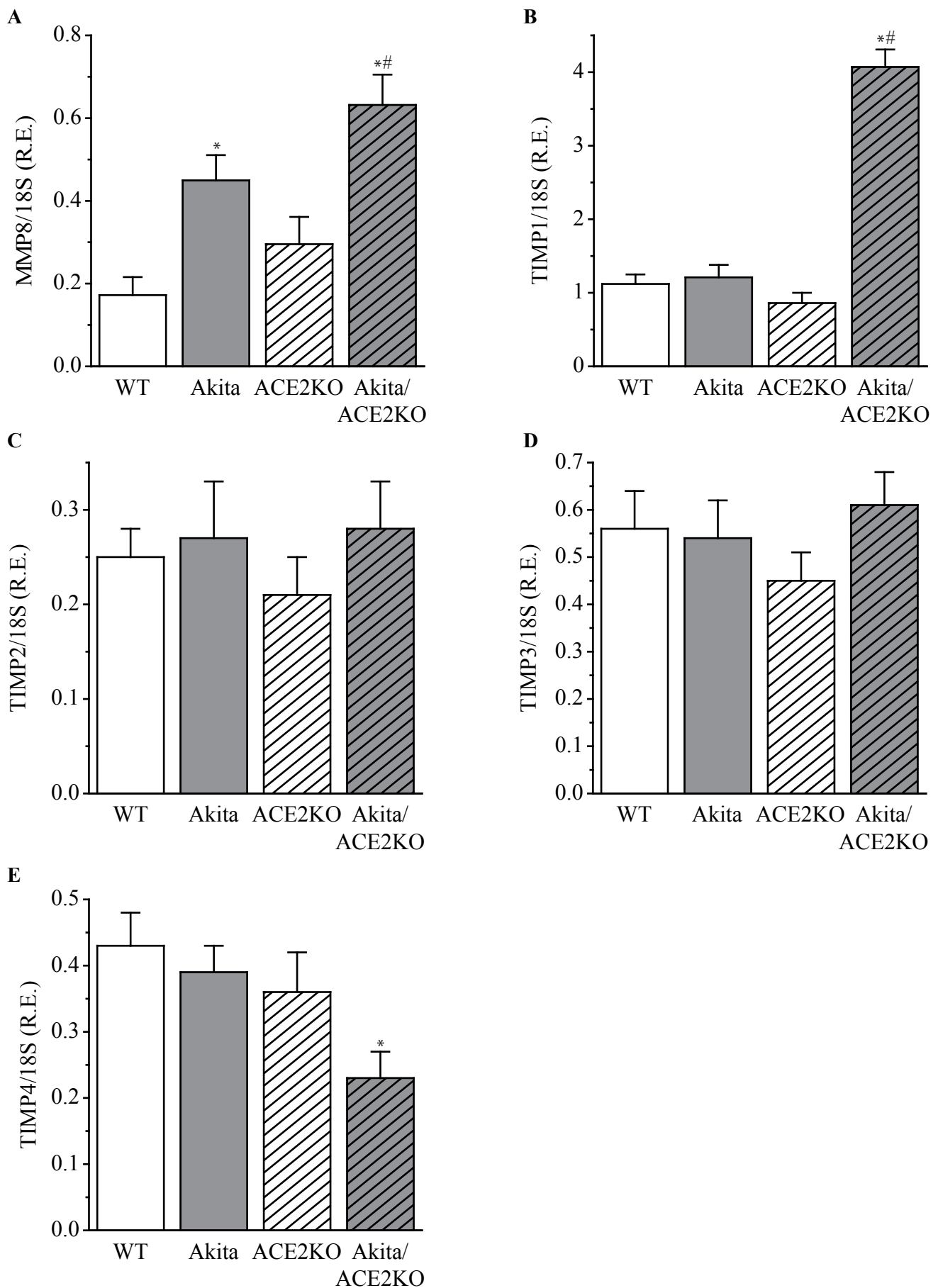
Supplemental Figure V. Taqman real-time PCR mRNA expression analysis showing elevated expression of matrix metalloproteinase (MMP)-8 (A) and tissue inhibitor of matrix metalloproteinase (TIMP)-1 (B) in Akita/ACE2KO hearts with no detectable change in TIMP2 (C) and TIMP3 (D) mRNA expressions within groups and decreased mRNA expression of TIMP4 (E) in Akita/ACE2KO hearts. R.E.=Relative Expression; n=10 per group. $*p < 0.05$ for the main effects and $\#p < 0.05$ for the interaction using two-way ANOVA.
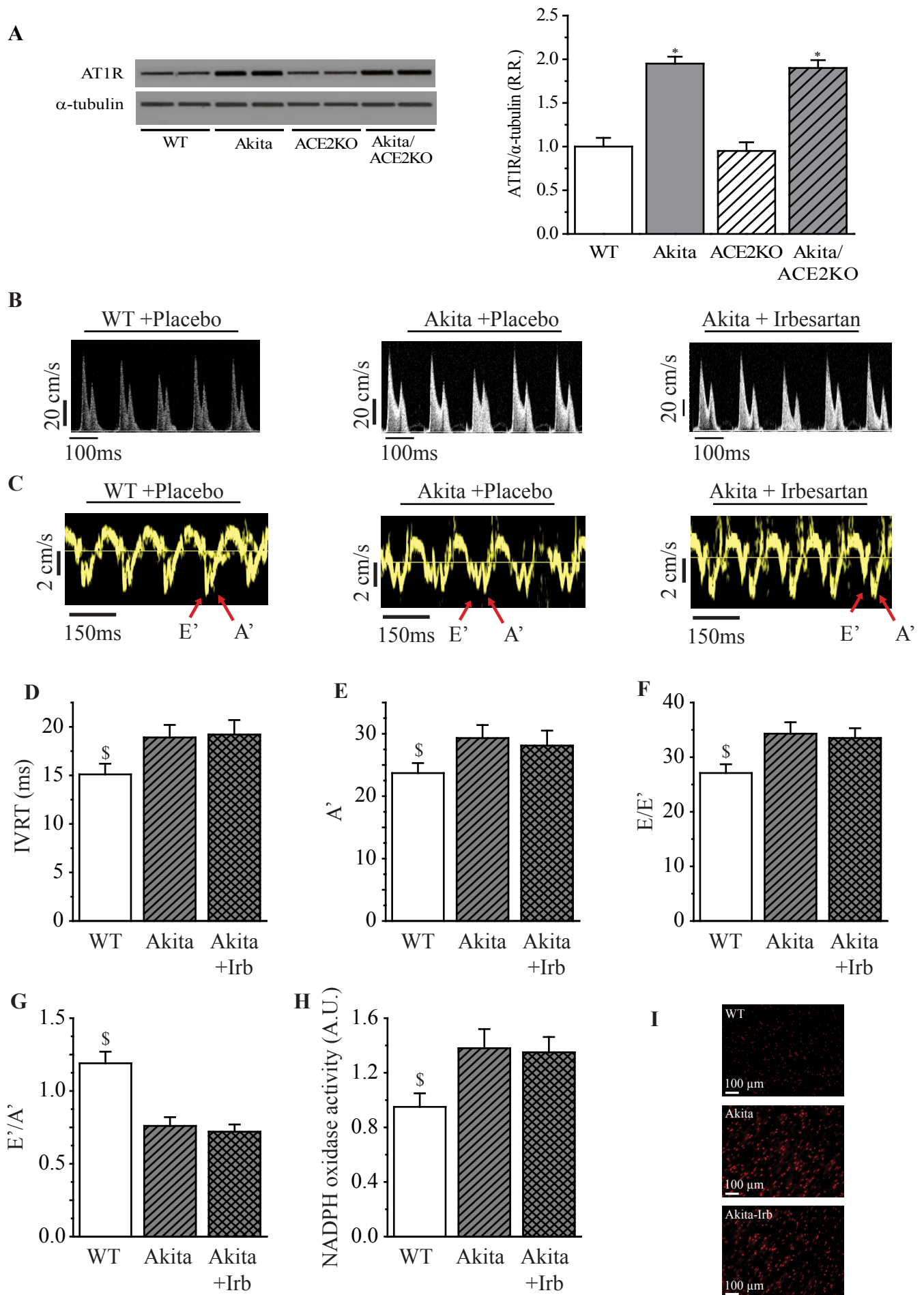
Supplemental Figure VI. Western blot analysis of myocardial AT1 receptor (A) showing increased AT1 receptor levels in Akita and Akita/ACE2KO hearts (n=5). Echocardiographic assessment of heart function using transmitral flow pattern (A) and tissue Doppler imaging (B) showing diastolic dysfunction in Akita hearts with lack of attenuation of dysfunction following AT1 receptor blocker, irbesartan. Quantitative evaluation of diastolic function showing increase in isovolumic relaxation time (IVRT) (D), A' wave velocity (A') (E), E/E' ratio (F) and decrease in E'/A' ratio (G) in Akita mice compared to WT mice, which was not restored after the treatment with irbesartan. Irbesratan also failed to suppress the elevated NADPH oxidase activity (H) and superoxide production (I) in Akita hearts, n=12 for each group except for Akita+Irbesartan group where n=10. *p<0.05 for the main effects interaction using two-way ANOVA; $p<0.05 compared to all other groups.

13

A

B

C
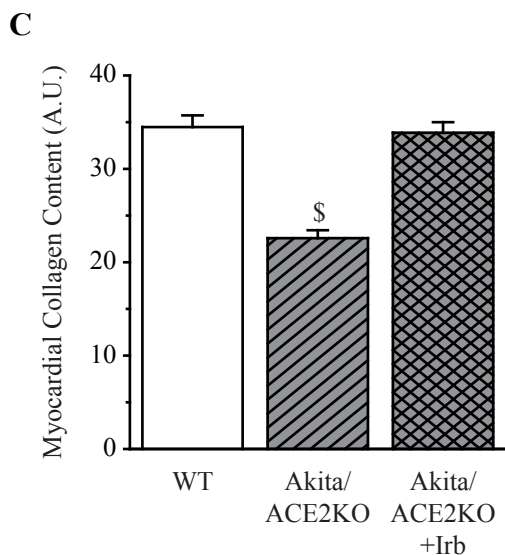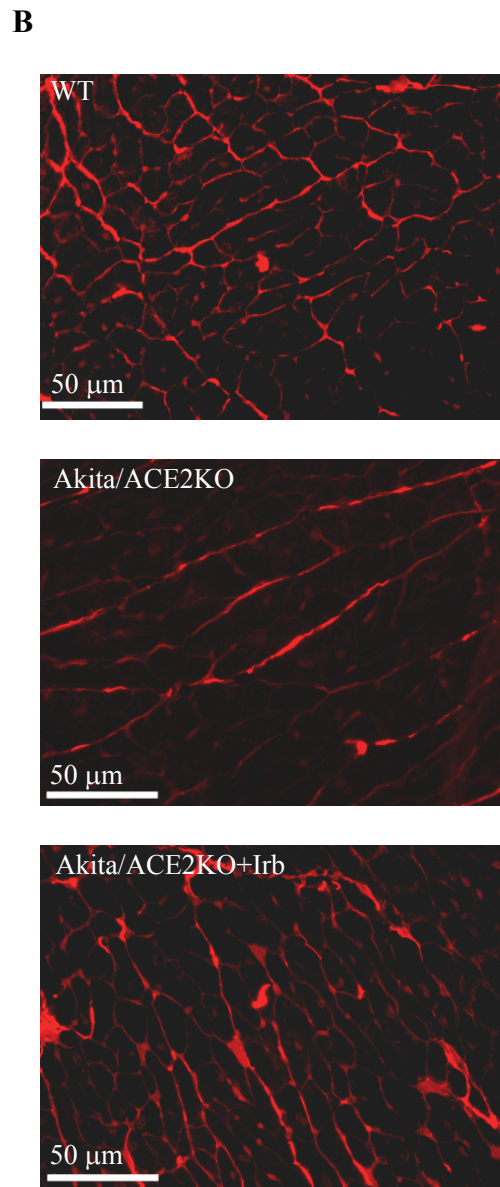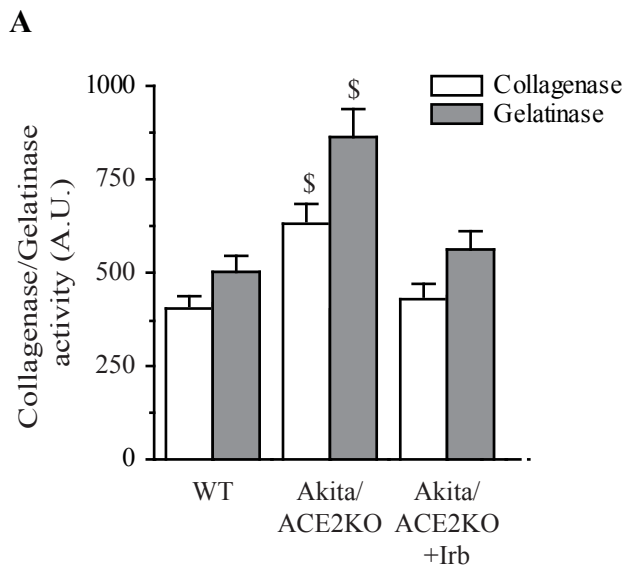
Supplemental Figure VII. Collagenase and gelatinase activities showing increased activity in Akita/ACE2KO hearts and normalization of activity upon treatment with irbesartan (n=10) (A). PSR staining images (B) and morphometric analysis of collagen content from PSR stained-images (n=3 sections per heart) (B) showing a restoration of the normal ECM architecture and increased collagen content in Akita/ACE2KO hearts in response to the AT1 receptor blocker, irbesartan (C) (n=5). A.U.=Arbitrary Unit; Irb=Irbesartan. $p<0.05 compared to all other groups.
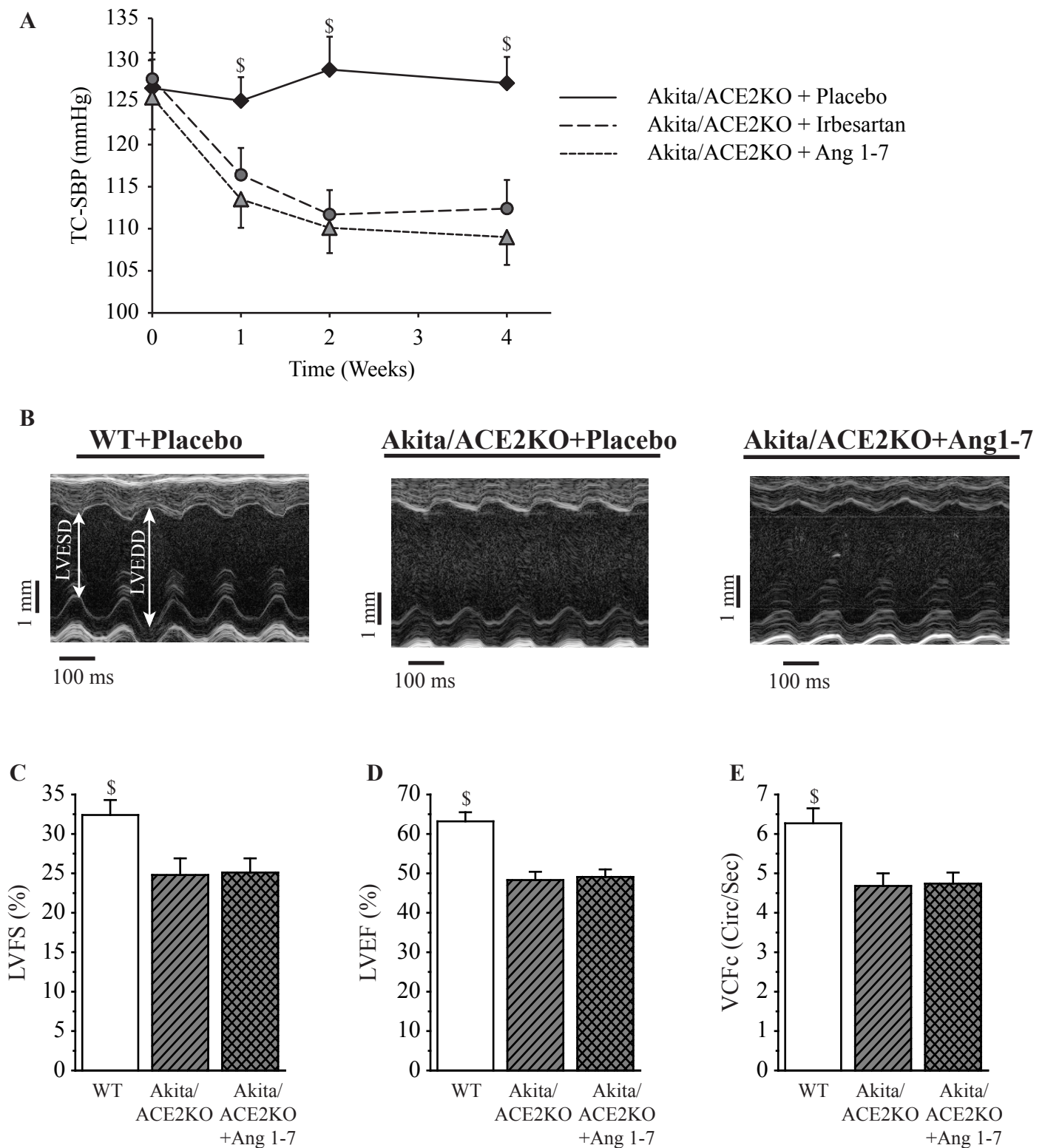
Supplemental Figure VIII. Mild hypertension in 6 months old Akita/ACE2KO mice and equivalent blood pressure lowering effects of irbesartan and angiotensin 1-7 (Ang 1-7) treatment in Akita/ACE2KO mice (A) based on tail-cuff systolic blood pressure (TC-SBP) measurements at various intervals. Echocardiographic assessment of heart function using M-mode images (B) showing systolic dysfunction in Akita/ACE2KO hearts with lack of a benefit in response to Ang 1-7 treatment. Quantitative evaluation of systolic function showing decreased LV fractional shortening (LVFS) (C), LV ejection fraction (LVEF) (D) and velocity of circumferential shortening (VCFc) (E) in Akita/ACE2KO hearts compared to WT hearts; Ang 1-7 treatment failed to normalize the systolic dysfunction in Akita/ACE2KO hearts. n=12 for each group except for Akita/ACE2KO+Ang 1-7 group where n=10. $p<0.05$ compared to all other groups.